SOLID-STATE ^{17}O NMR AS A NEW PROBE TO STUDY ACYL-ENZYME INTERMEDIATES

by

Aaron W. Tang

A thesis submitted to the Graduate Program in Chemistry

in conformity with the requirements for

the degree of Master of Science

Queen's University

Kingston, Ontario, Canada

April 2016

Abstract

This thesis reports on a combined solid-state ^{17}O NMR and quantum mechanical study of three acyl-enzyme intermediates: *p*-N,N-dimethylaminobenzoyl-chymotrypsin (DAB-CHT), *trans-o*-methoxycinnamoyl-chymotrypsin (oMC-CHT), and *trans-p*-methoxycinnamoyl-chymotrypsin (pMC-CHT). At pH 7.8, the three acyl-enzyme intermediates were found to undergo hydrolysis (deacylation) with the following rate constants: DAB-CHT, $6.4 \pm 0.1 \times 10^{-6}$; oMC-CHT, $2.8 \pm 0.1 \times 10^{-4}$ s^{-1}; pMC-CHT, $8.5 \pm 0.3 \times 10^{-3}$ s^{-1}. Analysis of solid-state ^{17}O NMR spectra obtained under the magic angle spinning (MAS) condition at 21 T for the three acyl-enzyme intermediates yields the following isotropic chemical shift (δ_{iso}), quadrupolar coupling constant (C_Q), and asymmetry parameter (η_Q): DAB-CHT, $\delta_{iso} = 316 \pm 2$ ppm, $C_Q = 10.0 \pm 1$ MHz, $\eta_Q = 0.6 \pm 0.2$; oMC-CHT, $\delta_{iso} = 316 \pm 2$ ppm, $C_Q = 9.2 \pm 1$ MHz, $\eta_Q = 0.6 \pm 0.2$; and pMC-CHT, $\delta_{iso} = 316 \pm 2$, $C_Q = 7.0 \pm 0.5$ MHz, $\eta_Q = 0.8 \pm 0.2$. With the aid of quantum mechanical calculations, these ^{17}O NMR parameters were interpreted as to reflect the variations in hydrogen bonding interactions between the carbonyl (C=O) functional group of the acyl moiety and the two NH groups from the protein backbone in the so-called oxyanion hole. This work represents the first use of solid-state ^{17}O NMR spectroscopy to study acyl-enzyme intermediates and demonstrates the great potential of this new technique.

Acknowledgements

I would like to thank my supervisor, Dr. Gang Wu, for his patience, support and advice. I would also like to thank Dr. Xianqi Kong for his time and help throughout the project. His help with synthesis and sample preparation is much appreciated. My colleagues in the Wu lab had also lent their support and I extend my thanks to them.

I would like to thank all my friends, especially Christina Lamparter, for their support and encouragement.

Finally, I want to thank my parents for their continual belief and support.

Table of Contents

List of Figures

List of Tables

Chapter 1

Introduction

1.1 General Introduction

Nuclear magnetic resonance (NMR) spectroscopy is a powerful technique for studying biological molecules. Detailed information on chemical environment, spatial orientation, proximity, and dynamics of the NMR-active nuclei can be extracted with a variety of NMR experiments. This is particularly important for biomolecules, where hydrogen, carbon and nitrogen nuclei all have spin-1/2 isotopes: ^{1}H (natural abundance of 99.985%), ^{13}C (1.1%), and ^{15}N (0.366%). For proton and carbon, the natural abundances of NMR-active isotopes are sufficient to obtain high-quality NMR spectra without isotopic enrichment. As a result, ^{1}H NMR and ^{13}C NMR are commonplace in studies of both small molecules and macromolecules.

Oxygen, the remaining underutilized element frequently found in biomolecules, is unique in that its only NMR-active isotope, ^{17}O, has very low natural abundance (0.037%). In addition, this isotope has a quadrupolar (spin-5/2) nucleus, therefore giving rise to broad NMR signals due to nuclear quadrupolar interactions. As a result, ^{17}O NMR has been an underutilized tool in analyzing biomolecules. However, oxygen is often intimately involved in the reaction centers of many enzyme-catalyzed reactions, for example, in carbonyl groups in esters and amides, and in hydroxyl groups in serine proteases. With a wide dispersion in chemical shifts – from 0 to 1600 ppm – for oxygen-containing functional groups,[1] ^{17}O NMR should be a sensitive probe of the chemical environment surrounding the oxygen atom.

There is an additional advantage in using ^{17}O NMR: as its quadrupolar nucleus is sensitive to the electric field gradient, ^{17}O NMR parameters will contain more information about the chemical environment around the nuclei than other spin-1/2 nuclei. NMR spectra recorded in the solid state will also provide more information than spectra recorded in solution, as chemical shift anisotropy is preserved and not averaged to the isotropic value.

The goal of the present project is to demonstrate the feasibility of using ^{17}O NMR as a probe to study biologically important reactions. As such, α-chymotrypsin was chosen for its well-known mechanism of catalysis and the wealth of available literature on the structure of its active site.

1.2 ^{17}O NMR

While there has been a considerable number of publications on ^{17}O NMR since the first absorption measurements of the oxygen nucleus by Alder and Yu,[2] the majority of published papers has focused on inorganic solids and liquids. Publications on chemical shifts and electric field gradient tensors in organic and biological compounds have only begun to be prevalent within the past two and a half decades.

1.2.1 ^{17}O NMR in Biological Systems

^{17}O NMR has been applied to a number of biologically relevant molecules. The first organic molecules to be analyzed via ^{17}O NMR were amino acids. Fiat and co-workers[3] obtained ^{17}O NMR spectra in ^{17}O-enriched monocrystalline α-glycine and polycrystalline L-alanine. Though poor spectral resolution led to ultimately inaccurate calculations of the ^{17}O NMR parameters, the study demonstrated the feasibility of

obtaining the respective electric field gradient and chemical shift tensors from the experimental solid-state ^{17}O NMR spectra.

Wu and Dong[4] reported ^{17}O multiple-quantum magic angle spinning (MQMAS) spectra for a number of organic solids, including D-alanine and D,L-glutamic acid-HCl. Interestingly, Lemaitre *et al*[5] later reported ^{17}O NMR spectra for D-glutamic acid-HCl and L-glutamic acid-HCl showing very different features from those previously reported. They attributed the spectral differences to conformational differences between racemic crystals of D,L-glutamic acid-HCl and chiral crystals of D-glutamic acid-HCl and L-glutamic acid-HCl, further suggesting that ^{17}O NMR parameters are very sensitive to non-covalent interactions.

Oldfield and co-workers[6] reported ^{17}O chemical shift tensor and quadrupolar coupling constant for the iron-dioxygen complex of the "picket fence" porphyrin analogue for oxymyoglobin and oxyhemoglobin. They observed averaging of the axially symmetric shielding tensor at room temperatures by anisotropic motion of the dioxygen ligand, and calculated a Fe-O-O bonding angle that is in agreement with previous X-ray crystallography studies.[7] The differences in ^{17}O NMR parameters observed between the bridging and terminal oxygen atoms were also in qualitative agreement with later density functional theory (DFT) calculations by Kaupp *et al*.[8]

The sensitivity of ^{17}O NMR parameters to the chemical environment has been demonstrated in nucleic acids as well. Wu *et al*[9] reported a systematic ^{17}O NMR study on all four nucleobases: thymine, uracil, cytosine, and guanine. They reported large differences in ^{17}O NMR parameters in seemingly similar functional groups and attributed these differences to the different degrees of hydrogen bonding in the molecular systems.

1.2.2 ^{17}O as a Probe for Hydrogen Bonding

Hydrogen bonding is ubiquitous in biological systems, and oxygen is optimally located in hydrogen bonds to probe for subtle changes in hydrogen bonding interactions. Though the relationship between ^{17}O NMR parameters and hydrogen bonding interactions is complex, many general trends can be observed.

Ando and co-workers[10] measured ^{17}O quadrupolar coupling constant ($C_Q = e^2qQ/h$), asymmetry parameter (η_Q), and chemical shift tensor in solid peptides and polypeptides, reporting that as the hydrogen bond length decreases, the quadrupolar coupling constant and chemical shift decrease. Later molecular orbital calculations showed the same trend.[11]

The amide group in organic molecules is also an important analogue to those found in peptides and some nucleic acids. Wu and co-workers[12] reported electric field gradient and chemical shielding tensors for benzamide, benzanilide, N-methylbenzamide, and acetanilide, revealing the same sensitivity of ^{17}O NMR parameters to intermolecular hydrogen bonding. This result is in agreement with previous ^{13}C NMR studies[13] on the effect of lengthening of the C=O bond length upon hydrogen bonding to the ^{13}C chemical shift tensor.

Hydrogen bonding in nucleic acids has also been examined by solid-state ^{17}O NMR. For example, Wu and co-workers[14] reported very different ^{17}O NMR tensors in the two carbonyl oxygen atoms in crystalline thymine due to different hydrogen bonding environments, even though the isotropic chemical shift are essentially the same.

Wu and co-workers reported a comprehensive experimental and theoretical study of C=O···H-N hydrogen bonds in crystalline urea.[15] They simulated the hydrogen bond

environment of urea using six models with increasing number of neighbouring urea molecules, with a range of zero to eight hydrogen bonds. They reported that as the number of hydrogen bonds increased, the quadrupolar coupling constant decreased, consistent with previous nuclear quadrupolar resonance (NQR) studies,[16-18] while the chemical shift decreased, following the general trend observed previously.[10-12]

1.2.3 Magic Angle Spinning (MAS)

NMR active nuclei interact with each other through nuclear dipolar interactions with a secular part of the Hamiltonian of the dipolar interaction taking the following form:

$$H = -\frac{1}{2} d\left[I_1 I_2 - 3I_{1Z} I_{2Z}\right]\left(3\cos^2\theta - 1\right) \quad (1)$$

where θ denotes the angle between the applied magnetic field and the vector connecting the two interacting nuclei.

In solutions, nuclei undergo rapid tumbling, and the dipolar interaction averages to zero, as the integral of $(3\cos^2\theta - 1)$ over a sphere is zero:

$$\int_0^{2\pi}\int_0^{2\pi} (3\cos^2\theta - 1)\sin\theta d\theta d\varphi = 0 \quad (2)$$

In the solid state, the dipolar interaction depends on θ, and can lead to significant line broadening and poorly resolved spectra. This was first demonstrated by the seminal paper by Pake in 1948.[19] The dipolar splitting of protons in the water molecules of $CaSO_4 \cdot H_2O$ single crystals was shown to vary as a function of θ, while for a powder sample the dipolar interactions give rise to a characteristic broad peak – the Pake doublet.

The technique of mechanical sample rotation to improve the resolution of NMR spectra was first independently developed by Andrew *et al*[20] and Lowe.[21] By rapidly

spinning the sample at the "magic angle" of 54.7° to the external applied magnetic field, chemical shift anisotropy, dipolar interactions, and first-order quadrupolar interactions are removed.

The first demonstration of MAS in ^{17}O NMR was reported by Oldfield *et al*. on inorganic solids,[22] and though the technique does not completely remove the second-order quadrupolar interaction, it provides a useful method of obtaining high-resolution spectra for ^{17}O nuclei in the solid state. In addition, since the residual second-order quadrupolar broadening in ^{17}O MAS spectra is inversely proportional to the applied magnetic field, it is beneficial to perform MAS at very high magnetic fields. In this Thesis, we use the combination of MAS and an ultrahigh magnetic field, 21 T, to obtain solid-state ^{17}O NMR spectra.

1.3 Enzyme Catalysis

1.3.1 Transition State Theory and Enzyme Catalysis

Although the catalytic action of enzymes had been noted since the nineteenth century,[23, 24] no conclusive theory of the mechanism of action was established until later in the twentieth century, when transition state theory began to be widely accepted over other competing hypotheses.[25]

The idea that enzymes act on molecules with specific geometry was most famously noted by Emil Fischer, in his seminal paper[26] on the influence of substrate configuration on enzymatic action, coining the popular analogy of "lock and key".[27] Three decades later J. B. S. Haldane amended the lock and key model to introduce the idea that enzymes induce certain strain to the substrates.[23] It was around this time when Henry Eyring published his statistical mechanical treatment of activated complexes[28] –

giving rise to what is now known as transition state theory. In this theory, chemical reactions occur when reactants collide and form a transition state, which can be described as a saddle point on a potential energy surface. The transition state is treated as being in equilibrium with the reactants, with a ratio between the two proportional to their free energy difference.

This framework was later applied to enzymes when Pauling[29] stated that enzymes have a complementary configuration to the activated complex, therefore having the greatest attraction to the transition state. A substrate, upon binding to the enzyme, will be deformed by the enzyme into the configuration of the transition state, thereby lowering the activation energy of the reaction and speeding up the reaction. Bernhard and Orgel[30] later reported serine protease inhibition by phosphate esters that imitate the tetrahedral transition state of the natural carbonyl substrate. They theorized that "hydrogen bonding and electrostatic interactions at or close to the ester linkage" was responsible for the much stronger binding for the transition state than the natural substrate. Studies on enzyme inhibition by using transition state analogues then became increasingly common.[31]

Further evidence for preferential binding to transition states was obtained when the first three-dimensional structure of hen egg-white lysozyme,[32] and the preliminary structure of lysozyme-inhibitor complexes[33] were determined via x-ray crystallography. The three dimensional structure suggested that upon binding the substrate was distorted from the normal chair conformation to a half-chair conformation. Later, this was extended to serine proteases, when a number of known inhibitors were found to resemble

the tetrahedral transition state of the substrate, and interact with the same "oxyanion hole" as does the substrate.[34, 35]

1.3.2 Mechanism of Catalysis in Serine Proteases

Chymotrypsin belongs to a group of enzymes known as serine proteases, named for a catalytically active nucleophilic serine residue in the active site. For chymotrypsin, the three catalytic residues - the "catalytic triad" – of serine-195, histidine-57, and aspartic acid-102 form a hydrogen-bond network in the binding pocket,[36] as illustrated in Figure 1.1. This hydrogen-bond network activates Ser195 for nucleophilic attack on the substrate, and along with the aforementioned oxyanion hole, provides the enzyme's catalytic power.

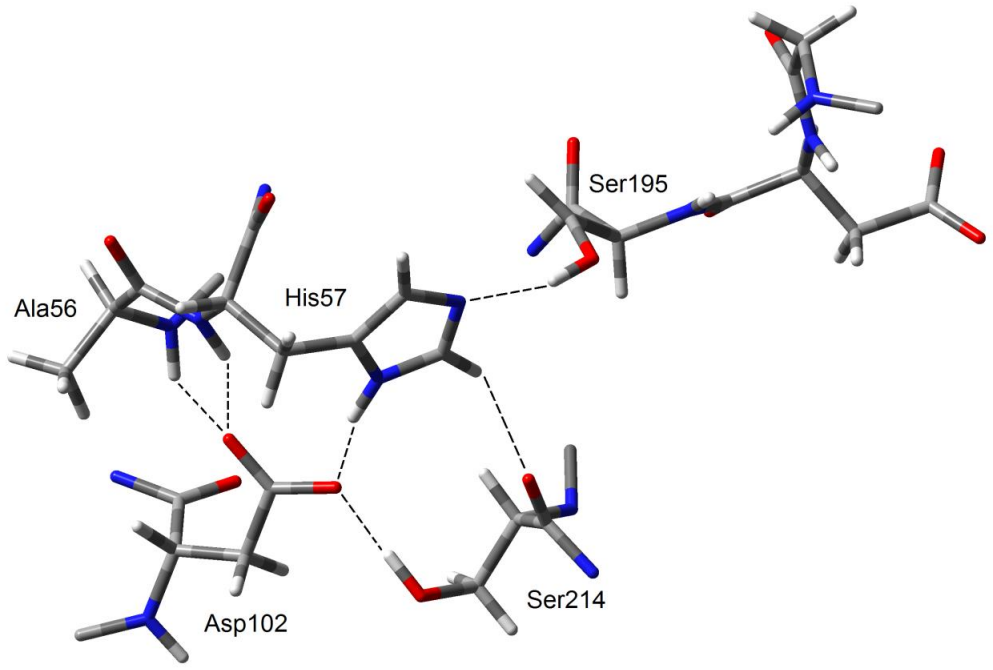

Figure 1.1: The hydrogen-bond network of the catalytic triad in α-chymotrypsin (PDB ID: 1YPH)

While the presence of the catalytic triad was first observed in a x-ray crystallography study by Blow *et al*,[37] the exact role of the amino acid residues in catalysis remained speculative. Direct observation of protons on His57 and Asp102 via ^{1}H NMR by Robillard *et al*[38] confirmed the proposed structure of the catalytic triad and revealed the hydrogen bond between the two amino acid residues. Later, Bachovchin and William[39] observed ^{15}N-^{1}H spin-spin coupling of labeled His57 residue with the Asp102 proton. The existence of the His57-Ser195 hydrogen bond has been a subject of debate, with initial crystallographic evidence suggesting that the residues are too far apart and not properly aligned for hydrogen bonding. Later, ^{15}N chemical shifts suggested the formation of a hydrogen bond in an acyl-enzyme transition state analogue.[40] Other heteronuclear NMR studies have been used to study serine proteases as well; Tsilikounas *et al*[41] used ^{11}B NMR to directly probe the geometry of boronic acid inhibitors. They showed the formation of a trigonal boron-histidine adducts, rather than a transition-state-like tetrahedral boron as previously thought.

Accompanying the catalytic triad is an oxyanion hole,[42] consisting of two hydrogen bond donors from the backbone of serine-195 and glycine-193, that stabilizes the oxygen on the scissile amide/ester bond in the tetrahedral transition state. The oxyanion hole is important for both the acylation and deacylation steps. The contribution of the oxyanion hole to catalysis is significant, as enzymes with the catalytic triad disabled via site-directed mutagenesis still retain hydrolytic activity with a reaction rate a thousand-fold higher than that for the uncatalyzed hydrolysis.[43]

The role of the oxyanion hole in transition state stabilization of the hydrolysis reaction was best illustrated with resonance Raman spectroscopy. Hydrogen bonds

between the backbone amides and the carbonyl oxygen increases the single-bond character of the C=O carbonyl bond, decreasing the observed stretching frequency. Tonge, Carey and co-workers[44] correlated the carbonyl stretching frequencies of a number of acyl-enzyme intermediates with the deacylation rates, thus providing evidence of transition state stabilization by hydrogen bonding in the oxyanion hole.

The enzyme catalyzes the hydrolysis reaction in two stages: 1) the acylation step where the substrate is covalently bonded to Ser195 to form the acyl-enzyme intermediate, breaking the amide or ester bond and releasing part of the substrate with the free amino terminus, and 2) the deacylation step where the ester bond in the acyl-enzyme intermediate is hydrolyzed; as illustrated in Figure 1.2. When the substrate contains a suitably stable leaving group, the formation of the acyl-enzyme occurs rapidly, and the hydrolysis of the acyl-enzyme is rate-limiting.[45]

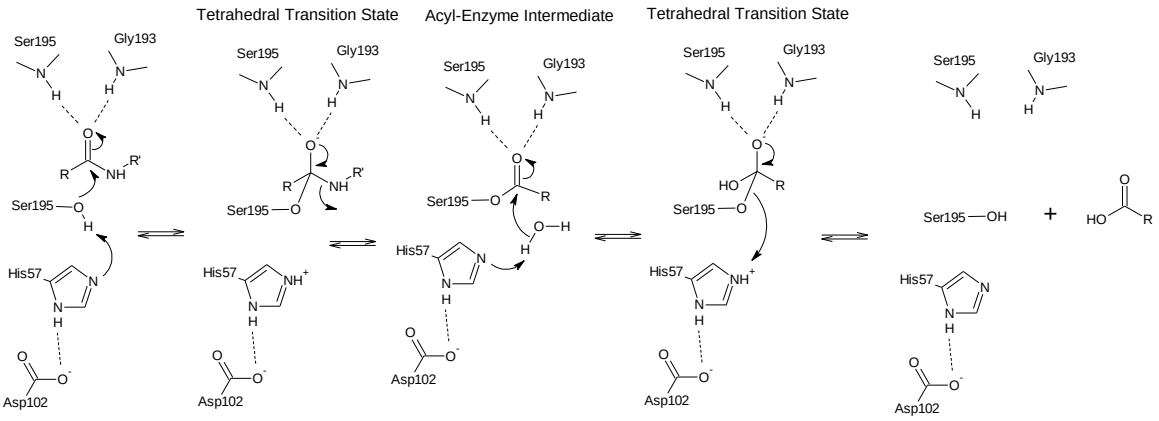

Figure 1.2: Accepted mechanism of serine protease catalysis. Figure adapted from Hedstrom.[36]

The steady-state kinetic treatment of the hydrolysis reaction catalyzed by chymotrypsin follows three steps: 1) the formation of the substrate-enzyme complex (ES), 2) the transesterification reaction that leads to the formation of the acyl-enzyme

intermediate (EP_2) and the release of the hydrolysis product (P_1), and 3) the hydrolysis of the acyl-enzyme intermediate.

$$E + S \underset{k_{-1}}{\overset{k_1}{\leftrightarrow}} ES \overset{k_2}{\rightarrow} EP_2 + P_1 \overset{k_3}{\rightarrow} E + P_2 \tag{3}$$

The reaction rates of the three steps are described by their respective rate constants, k_1, k_{-1}, k_2, and k_3. Under the assumption that step 3 is rate limiting, the hydrolysis of the acyl-enzyme is described by first order kinetics, with the rate law as follows:

$$\frac{d[P_2]}{dt} = k_3[EP_2] \tag{4}$$

While the reaction mechanism is well known, the acyl-enzyme intermediate and tetrahedral transition states are generally too transient for NMR studies. One strategy is to use a poor substrate with a good leaving group that rapidly acylates the enzyme active site following the mechanism outlined above, but remains covalently bonded for a significant amount of time. With a long deacylation half-life, the acyl-enzyme intermediate can be isolated and studied via NMR.

1.4 Objectives of the Thesis

Our central hypothesis in this thesis is that, as the acyl carbonyl oxygen atom is at the centre of the oxyanion hole, ^{17}O NMR parameters should be sensitive to the molecular interactions that are key to catalysis. To test this hypothesis, we synthesized a series of ^{17}O-labled chymotrypsin substrates with different hydrolysis kinetics, then prepared acyl-enzyme intermediates, and finally performed solid-state ^{17}O NMR experiments to obtain the ^{17}O NMR parameters. To fully explore the relationship between ^{17}O NMR parameters and the hydrogen bonding interaction in the oxyanion hole in the

serine proteases, we employed quantum chemical calculations to map out the NMR parameter surface, which provides a means of interpreting the experimental ^{17}O NMR results.

Chapter 2

Experimental Methods

In this thesis, four chymotrypsin substrates/inhibitors with varying deacylation kinetics were studied: *p*-N,N-dimethylaminobenzoylimidazole (DAB-Im), *trans-o*-methoxycinnamoylimidazole (oMC-Im), *trans-p*-methoxycinnamoylimidazole (pMC-Im), and *trans*-cinnamoylimidazole (C-Im) (Figure 2.1).

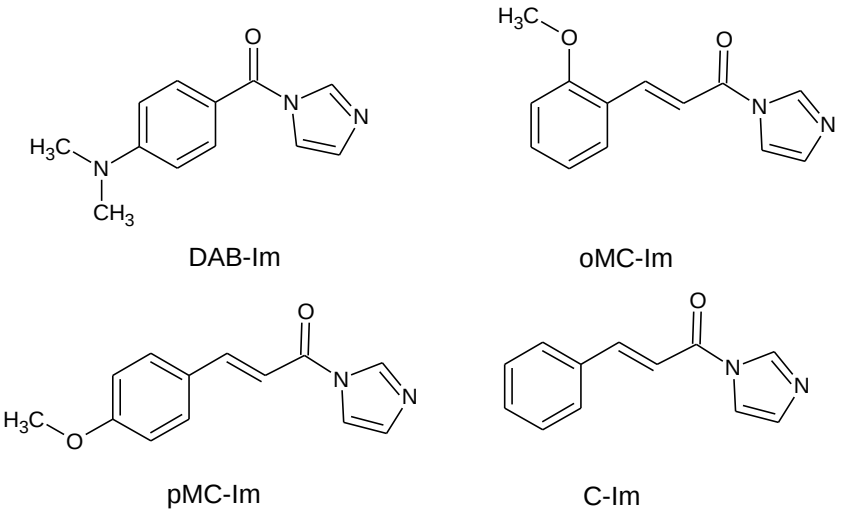

Figure 2.1: Structure of the four chymotrypsin substrates/inhibitors.

2.1 Synthesis of ^{17}O-Enriched Substrates

2.1.1 [1,2-$^{17}O_2$]Cinnamic acids

Trans-o-methoxycinnamic acid and *trans-p*-methoxycinnamic acid were synthesized via Knoevengal condensation of the corresponding benzaldehydes with ^{17}O-labelled malonic acid (Reaction Scheme 1).

Reaction Scheme 1

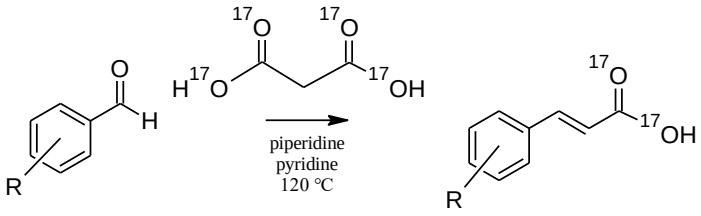

R = **2** *o*-OCH_3
3 *p*-OCH_3

***trans-o*-methoxycinnamic acid.** *o*-methoxybenzaldehyde (281 mg, 2.06 mmol) and ^{17}O-labelled malonic acid (400 mg, 3.84 mmol, 1.87 mol equiv) were placed in a 10 mL round bottom flask, to which piperidine (162 µL) and pyridine (3.24 mL) was added. The reaction mixture was refluxed in an oil bath at 120 °C for 3 hours. The solvent was evaporated under reduced pressure at 50 °C until a light yellow liquid remained, which was then transferred to a small beaker with ethanol. The solution was acidified with HCl (3.24 mL), and the final product precipitated with the addition of cold H_2O (13.5 mL). The insoluble white product was collected via suction filtration, then washed with cold H_2O (3 × 3 mL) and hexanes (2 × 2mL) to yield 0.311 g (84.6%) of final product. ^1H NMR (500 MHz, acetone-d6) δ 7.98 (d, J = 16.2 Hz, 1H), 7.66 (dd, J = 7.6, 1.3 Hz, 1H),

7.4 (ddd, *J* = 8.4, 7.3, 1.3 Hz, 1H), 7.08 (d, *J* = 8.4 Hz, 1H), 6.99 (t, *J* = 7.4 Hz, 1H), 6.54 (d, *J* = 16.1 Hz, 1H), 3.92 (s, 3H); ^{17}O NMR (67.7 MHz, acetone-d6) δ 251.79 (s, 1O).

2.1.2 Imidazole derivatives

To yield the imidazole derivative, the corresponding acids were coupled to imidazole using N,N'-carbonyldiimidazole (CDI), a common coupling reagent (Reaction Scheme 2).

Reaction Scheme 2

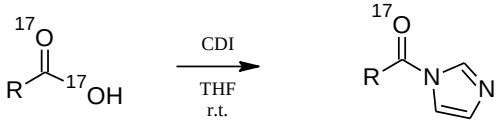

R = **1** *p*-((CH$_3$)$_2$N)(C$_6$H$_4$)-
2 *o*-(CH$_3$O)(C$_6$H$_4$)(HC=CH)-
3 *p*-(CH$_3$O)(C$_6$H$_4$)(HC=CH)-
4 (C$_6$H$_5$)(HC=CH)-

***p*-N,N-dimethylaminobenzoylimidazole (DAB-Im)**. ^{17}O-labelled *p*-N,N-dimethylaminobenzoic acid (100.0 mg, 0.6054 mmol) and CDI (148.6 mg, 0.9164 mmol, 1.514 mol equiv) were added to a 10 mL round bottom flask, which was then capped with a rubber septum. The headspace was purged with nitrogen gas with a needle for 1 minute, and anhydrous THF (3 mL) was added with a syringe and needle. Some insoluble grey/blue solids remained. The headspace was again purged with nitrogen gas for 5 minutes. The reaction mixture was stirred for 19 hours, after which insoluble solid remained visible. The solvent was removed under reduced pressure until a light-grey oil and solid remained. The residue was transferred to an extraction funnel with $CHCl_3$ (2 × 2 mL). The organic layer was washed with $NaHCO_3$ solution (2 × 2 ml 0.8% w/v),

saturated Na_2SO_4 solution (3 mL), then dried (Na_2SO_4). The organic solvent was removed under reduced pressure until a light grey/purple solid remained. The residue was dissolved in $CHCl_3$ (2 mL), and some activated charcoal was added. The mixture was filtered through a Pasteur pipette with a cotton plug, packed with a layer of celite. The pipette was rinsed with $CHCl_3$ (2 mL, 1 mL). The eluent was light purple, and the solvent was removed under reduced pressure. The off-white residue was dried under vacuum overnight. The residue was dissolved in acetone (1.5 mL) and precipitated with cold H_2O (8 mL), forming a white, flocculent solid. The solid was collected via suction filtration, and washed with cold H_2O (2 × 4 mL) and hexanes (2 × 2 mL) to yield 47.5 mg (36.5%) of final product **1**. ^{1}H NMR (400 MHz, acetone-d6) δ 8.09 (s, 1H), 7.77 (dt, J = 9.2, 2.2 Hz, 2H), 7.58 (t, J = 1.38 Hz, 1H), 7.10 (d, J = 0.5 Hz, 1H), 6.87 (dt, J = 9.1, 2.2 Hz, 2H), 3.14 (s, 6H); ^{17}O NMR (54.1 MHz, acetone-d6) δ 410.36 (br, s, 1O).

***trans*-*o*-methoxycinnamoylimidazole (oMC-Im).** *trans*-*o*-methoxycinnamic acid (200 mg, 1.12 mmol) and CDI (303 mg, 1.87 mmol, 1.67 mol equiv) were added to a 10 mL round bottom flask. Anhydrous THF (4 mL) was added and the flask was sealed with a rubber septum stopper. The headspace of the flask was purged with nitrogen gas introduced with a needle. The reaction mixture was stirred for 13 hours. The solvent was evaporated under reduced pressure. Crude product was dissolved in DCM (5 mL) and toluene (15 mL), and washed with $NaHCO_3$ solution (2.5 mL 0.8% w/v), saturated Na_2SO_4 solution (3 × 3 mL). The organic layer was dried (Na_2SO_4), then the solvent was removed to yield a crude solid product. The residue was recrystallized from acetone (14 mL) and cold H_2O (50 mL), then washed with cold H_2O (3 × 10 mL) to yield 181 mg (70.7%) of final product **2.** ^{1}H NMR (500 MHz, acetone-d6) δ 8.54 (s, 1H), 8.38 (d, J =

15.6 Hz, 1H), 7.92 (dd, *J* = 7.7, 1.6 Hz, 1H), 7.82 (t, *J* = 1.3 Hz, 1H), 7.61 (d, *J* = 15.6 Hz, 1H), 7.50 (ddd, *J* = 8.7, 6.9, 1.6 Hz, 1H), 7.15 (d, *J* = 8.5 Hz, 1H), 7.10 (s, 1H), 7.05 (t, *J* = 7.57 Hz, 1H), 3.99 (s, 3H); ^{17}O NMR (67.7 MHz, acetone-d6) δ 384.53 (br, s, 1O).

***trans*-*p*-methoxycinnamoylimidazole (pMC-Im)** was prepared by Dr. Xianqi Kong. *trans*-*p*-methoxycinnamic acid (200 mg, 1.12 mmol) and CDI (303 mg, 1.87 mmol, 1.67 mol equiv) were added to a 10 mL round bottom flask. Anhydrous THF (4 mL) was added and the flask was sealed with a rubber septum stopper. The headspace of the flask was purged with nitrogen gas introduced with a needle. The reaction mixture was stirred for 13 hours. The solvent was evaporated under reduced pressure. Crude product was dissolved in DCM (5 mL) and toluene (15 mL), and washed with $NaHCO_3$ solution (2.5 mL 0.8% w/v), saturated Na_2SO_4 solution (3 × 3 mL). The organic layer was dried (Na_2SO_4), then the solvent was removed to yield a crude solid product. The residue was recrystallized from acetone (14 mL) and cold H_2O (50 mL), then washed with cold H_2O (3 × 10 mL) to yield the final product **3.**

***trans*-cinnamoylimidazole (C-Im).** ^{17}O-labelled *trans*-cinnamic acid (67.7 mg, 0.457 mmol) and CDI (140 mg, 0.863 mmol, 1.89 mol equiv) were added to a 10 mL round bottom flask. Anhydrous THF (2 mL) was added to the flask, which was then sealed with a rubber septum. The headspace was purged with nitrogen gas via a needle. The reaction mixture was stirred for 17 hours. The solvent was removed under reduced pressure, until a small amount of colourless liquid remained. The liquid was transferred to an extraction funnel with DCM (2 × 2.5 mL) and hexanes (2 × 7.5 mL). The organic layer was washed with $NaHCO_3$ solution (3 × 2 mL 0.8% w/v), saturated Na_2SO_4 solution (3 mL), and then dried (Na_2SO_4). The remaining organic solvent was removed under reduced pressure at

40 °C until white solid remained. The residue was recrystallized from acetone and cold H_2O to yield 38.4 mg (42.4%) of white product **4**. ^{1}H NMR (500 MHz, acetone-d6) δ 8.59 (s, 1H), 8.06 (d, J = 15.4 Hz, 1H), 7.90 (dd, J = 7.3, 2.0 Hz, 2H), 7.85 (s, 1H), 7.64 (d, J = 15.6 Hz, 1H), 7.55-7.47 (comp, 3H), 7.11 (s, 1H); ^{17}O NMR (67.7 MHz, acetone-d6) δ 388.34 (br, s, 1O).

2.2 Formation of the Acyl-Enzyme Intermediates

The acyl-enzyme intermediate was formed via acyl transfer of the imidazole derivative to the hydroxyl residue in serine-195 of α-chymotrypsin (Reaction Scheme 3). The reaction is driven by the departure of the imidazole leaving group.

Reaction Scheme 3

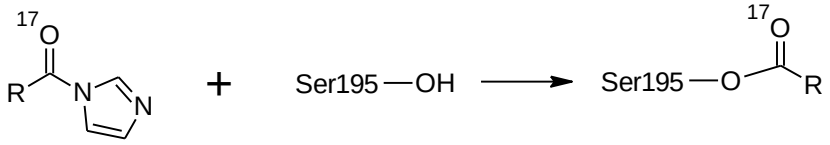

R = **1** *p*-((CH$_3$)$_2$N)(C$_6$H$_4$)-
2 *o*-(CH$_3$O)(C$_6$H$_4$)(HC=CH)-
3 *p*-(CH$_3$O)(C$_6$H$_4$)(HC=CH)-
4 (C$_6$H$_5$)(HC=CH)-

***p*-N,N-dimethylaminobenzoylchymotrypsin (DAB-CHT).** α-chymotrypsin (50.1 mg) was dissolved in acetate buffer (1 mL 0.1 M, pH 4.00) in a 2.5 mL Eppendorf microcentrifuge tube. *p*-N,N-dimethylaminobenzoylimidazole (4.4 mg, 10 mol equiv) was dissolved in acetonitrile (100 μL). The two solutions were mixed and allowed to react for 30 minutes. Four 1 mL plastic syringes were plugged with glass wool and packed with Sephadex G-25. The reaction mixture was split into four 275 μL fractions

and added to the syringes, which were then centrifuged briefly. The eluent fractions were combined and immediately frozen in a dry ice/acetone bath, and lyophilized overnight to yield 39.1 mg (77%) of solid product. MS (ESI-ion trap) mass: Calcd 25597; Found 25597.

***trans*-*o*-methoxycinnamoylchymotrypsin (oMC-CHT).** α-chymotrypsin (25.3 mg) was dissolved in acetate buffer (1 mL 0.1 M, pH 4.00) in a 2.5 mL Eppendorf microcentrifuge tube. *trans*-*o*-methoxylcinnamoylimidazole (3.8 mg) was dissolved in acetonitrile (165.2 μL). 100 μL (10 mol equiv) of the above solution was added to the enzyme and allowed to react for 1 minute. Four 1 mL plastic syringes were plugged with glass wool and packed with Sephadex G-25. The reaction mixture was split into four 275 μL fractions and added to the syringes, which were then centrifuged briefly. The eluent fractions were combined and immediately frozen in a dry ice/acetone bath, and lyophilized overnight to yield 20.6 mg (81%) of solid product. MS (ESI-ion trap) mass: Calcd 25610; Found 25610.

***trans*-*p*-methoxycinnamoylchymotrypsin (pMC-CHT).** α-chymotrypsin (25.1 mg) was dissolved in acetate buffer (1 mL 0.1 M, pH 4.00) in a 2.5 mL Eppendorf microcentrifuge tube. *trans*-*p*-methoxylcinnamoylimidazole (2.8 mg, 12 mol equiv) was dissolved in acetonitrile (100 μL). The two solutions were mixed and allowed to react for 1 minute. Four 1 mL plastic syringes were plugged with glass wool and packed with Sephadex G-25. The reaction mixture was split into four 275 μL fractions and added to the syringes, which were then centrifuged briefly. The eluent fractions were combined and immediately frozen in a dry ice/acetone bath, and lyophilized overnight to yield 20.1 mg (80%) of solid product. MS (ESI-ion trap) mass: Calcd 25610; Found 25610.

***trans*-cinnamoylchymotrypsin (C-CHT).** α-chymotrypsin (50.3 mg) was dissolved in acetate buffer (1 mL 0.1 M, pH 4.00) in a 2.5 mL Eppendorf microcentrifuge tube. *trans*-cinnamoylimidazole (4.2 mg, 11 mol equiv) was dissolved in acetonitrile (100 μL). The two solutions were mixed and allowed to react for 1 minute. Four 1 mL plastic syringes were plugged with glass wool and packed with Sephadex G-25. The reaction mixture was split into four 275 μL fractions and added to the syringes, which were then centrifuged briefly. The eluent fractions were combined and immediately frozen in a dry ice/acetone bath, and lyophilized overnight to yield 39.1 mg (77%) of solid product. MS (ESI-ion trap) mass: Calcd 25580; Found 25580.

2.3 Mass Spectrometry

Formation of covalently bonded acyl-enzyme was confirmed via mass spectrometry. Mass spectra were recorded by Dr. Jiaxi Wang on a Thermo Scientific Orbitrap Velos Pro mass spectrometer with electrospray ionization in positive ion mode. Deconvolution was performed using Thermo Scientific ProMass, under positive ion mode with adduct ion mass of 1.0079 Da. The output mass range was set to 20,000 Da to 80,000 Da, the default setting for large proteins.

2.4 Kinetic Measurements with Chymotrypsin Activity Assay

The activity of chymotrypsin was measured with a chymotrypsin activity assay adopted from the testing protocol of Sigma-Aldrich,[46] where the enzyme-catalyzed hydrolysis of N-benzoyl-L-tyrosine ethyl ester (BTEE) was tracked via UV-vis spectroscopy.

A solution of 80 mM Tris buffer was prepared by dissolving 9.69 mg/mL Tris-base, then pH brought to 7.80. The 1.18 mM BTEE solution was prepared by dissolving

18.5 mg BTEE in 31.7 mL methanol, and filled to the mark with water in a 50 mL volumetric flask. A 2 M $CaCl_2$ solution was prepared by dissolving 221.96 mg/mL anhydrous $CaCl_2$. 1 mM HCl solution was prepared by serial dilution from concentrated HCl.

The enzyme solution was prepared by dissolving enough chymotrypsin (approximately 30-80 μg) in 1 mM HCl to reach approximately 2-5 units/mL (1 unit is defined as 1 μmole BTEE consumed per minute at pH 7.80 at 25°C). Then 1.420 mL of Tris buffer, 1.400 mL of BTEE, and 80 μL of $CaCl_2$ solutions were mixed in a quartz cuvette and equilibrated at 25°C. 100 μL of the enzyme solution was added to the cuvette, which was inverted five times. UV-vis spectra were recorded immediately with a Jasco J-815 CD spectrometer using time course measurement at 256 nm over 3-5 minutes (slit width = 2500 nm).

The measurement with the acyl-enzyme intermediate is identical to the above description, except a stock solution of acyl-enzyme was made from the lyophilized products as described in section 2.2. Activity readings were taken using aliquots from the stock solution at 1.5, 8.5, 14.5, 23, 39, and 47 hour time points. The assay in each time point was done in triplicate. The percentage of chymotrypsin inhibited is calculated by comparing the activity of the acyl-enzyme solution at each time point against that of a control solution of α-chymotrypsin that has been prepared concurrently to account for the natural degradation of enzyme activity over time.

2.5 Kinetic Measurements with UV-Vis Spectroscopy

Hydrolysis rates of various acyl-enzymes were tracked via a Jasco J-815 CD spectrometer. The acyl-enzyme solution was prepared by dissolving 1.5 mg lyophilized

acyl-chymotrypsin intermediate in 3 mL buffer (80 mM Trizma, 50 mM $CaCl_2$, pH 7.80) in a quartz cuvette. UV-vis spectrum was recorded over wavelengths of 250-350 nm (slit width = 100 μm, data pitch = 0.1 nm, scanning speed = 100 nm/min), with sample cell kept at 25.0 °C. The data collection time points ranged between a period of 120 hours for DAB-CHT, 210 minutes for oMC-CHT, and 10 minutes for pMC-CHT. The last reading for each inhibitor is treated as the baseline against which a difference spectrum can be calculated, as enough time has passed to assume that hydrolysis of the acyl-enzyme complex is complete.

2.6 NMR Studies

Synthetic products were characterized using solution-state NMR obtained with Bruker AVANCE-300, AVANCE-400, and AVANCE-500 NMR spectrometers. Solid-state ^{17}O MAS NMR spectra were obtained with a 900 MHz Bruker Avance II NMR spectrometer by Dr. Victor Terskikh at the National Ultrahigh-Field NMR Facility for Solids. Spectra simulations were performed with *Dmfit.*[47]

2.7 Computational Study

^{17}O NMR parameters were calculated with *Gaussian 09* on High Performance Computing Virtual Laboratory (HPCVL) servers. The calculations were performed on Becke-3-Parameter, Lee-Yang-Parr (B3LYP) level of theory, with the 6-311++g(d,p) basis set. The calculated NMR parameters were calibrated with experimentally obtained data from methyl *p*-methoxycinnamate (pMC-Me) as previously done:[15, 48] the nuclear quadrupolar moment of oxygen (Q) was adjusted from -2.558 fm^2 to -2.305 fm^2 such that the calculated quadrupolar coupling constant ($C_Q = eQq_{zz}/h$) matches the experimental figure, and the absolute shielding constant (σ) was adjusted from 287.5 ppm to 270.2

ppm such that the calculated isotropic chemical shift ($\delta_{iso} = \sigma - \sigma_{iso}$) matches the experimentally obtained figure.

Chapter 3

Results and Discussion

We first confirmed via mass spectrometry the successful synthesis of acyl-chymotrypsin intermediates. The dissociation kinetics of the acyl-chymotrypsin intermediates were then studied and corroborated against literature values. Solid-state ^{17}O-NMR spectra were then obtained, and the NMR parameters were analyzed against known trends. Finally, computational studies were performed with a number of models to examine how the different NMR parameters were affected by hydrogen bonding.

3.1 Mass Spectra of Acyl-Enzyme Intermediates

To confirm the formation of covalently bonded acyl-enzyme intermediates in the reaction between α-chymotrypsin and substrates, the synthetic products were analyzed via electrospray ionization-ion trap mass spectrometry (ESI-MS). The experimental mass spectra for the four acyl-enzymes intermediates are shown in Figure 3.1 and the measured masses are summarized in Table 3.1.

Table 3.1: Experimental and theoretical MS data and degree of acylation of the acyl-enzyme intermediates.

Acyl-Enzyme	Chymotrypsin	Acyl-Enzyme Intermediate		% Acyl-Enzyme
	Experimental Mass	Theoretical Mass*	Experimental Mass	
DAB-CHT	25444.7 ± 8.0	25591.9 ± 8.0	25597.2 ± 1.5	92
oMC-CHT	25449.2 ± 0.3	25609.4 ± 0.3	25608.9 ± 0.3	87
pMC-CHT	25449.2 ± 0.7	25609.4 ± 0.7	25609.7 ± 0.6	79
C-CHT	25449.7 ± 1.4	25579.8 ± 1.4	25579.7 ± 0.3	95

* In each case, the theoretical mass of the acyl-enzyme intermediate was calculated by adding the experimental mass of chymotrypsin and the molecular mass of the acyl moiety.

In the mass spectrum of pMC-CHT (shown in Figure 3.1c), there is a major component at M = 25609.7 Da corresponding to pMC-CHT, and a minor component at M = 25449.2 Da corresponding to free chymotrypsin. The experimental mass difference between the two components is 160.5 ± 0.4 Da, consistent with the theoretical difference of 160.2 Da. This observation confirms the integrity of the acyl-enzyme intermediate. The mass spectra for the other acyl-enzymes exhibit very similar features. On the basis of the peak areas of the acyl-enzyme and free enzyme, we estimated the level of acylation at the time of measurement to be in a range from 79% to 95% for the four acyl-enzyme products, as shown in Table 3.1. These are very satisfactory results.

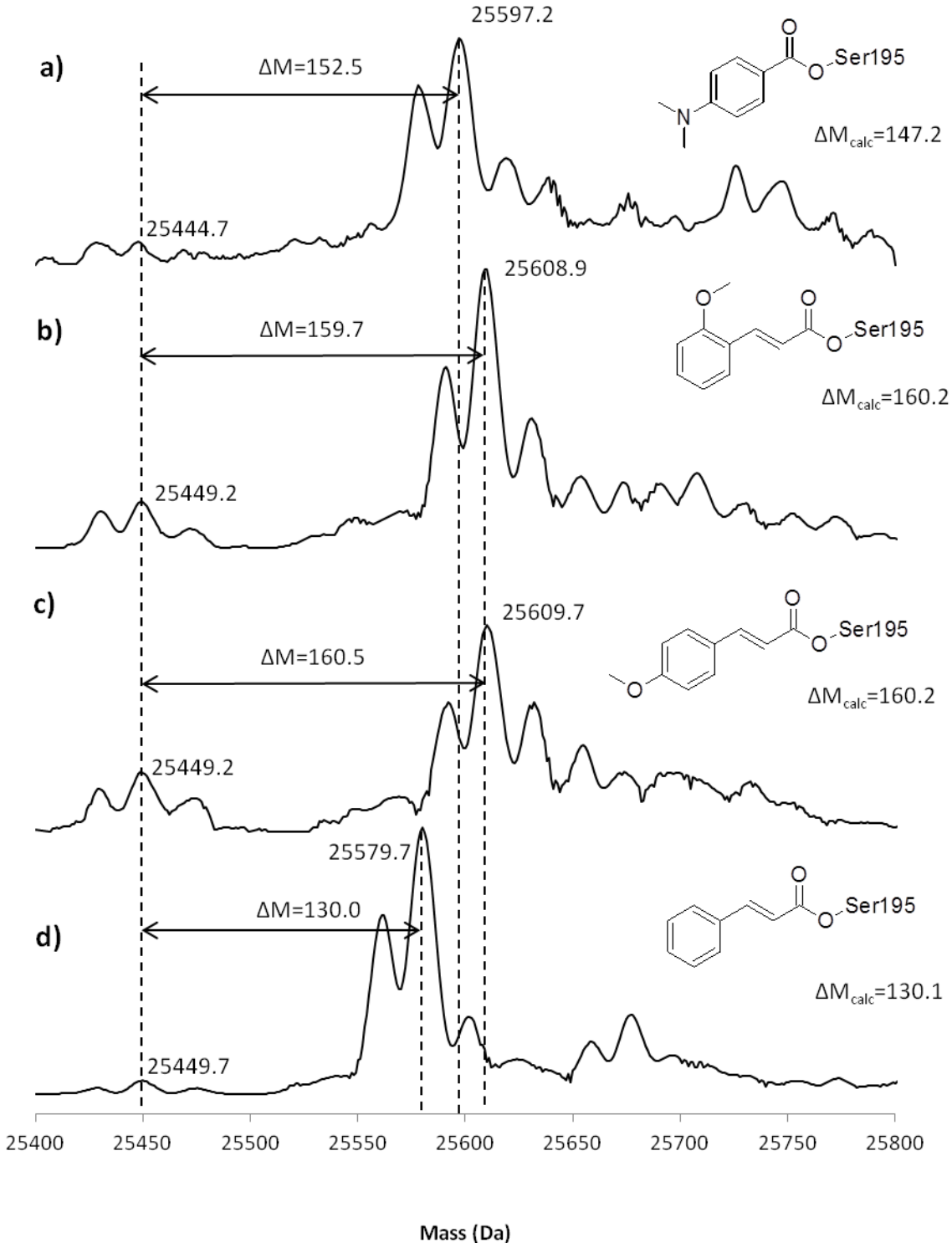

Figure 3.1: Deconvoluted mass spectra of acyl-enzyme intermediates: a) DAB-CHT, b) oMC-CHT, c) pMC-CHT, d) C-CHT.

Ashton *et al*[49] have previously studied the formation of O-acyl chymotrypsin intermediates using ESI-MS, reporting the presence of two mass components for α-chymotrypsin, a major component at 25,450 Da, and a minor component at 25,237 Da. They reported a mass of 25,580 Da for the major component of C-CHT, in agreement with our measured mass of 25,579.7 ± 0.3 Da. Later studies[50] revealed that the chymotrypsin components were two of the seven isoforms that result from the activation of chymotrypsinogen A, and differed only by two amino acid residues. The minor component (α-chymotrypsin) resulted from the cleavage of the peptide bond between amino acids 148-149 in the major component (α_1-chymotrypsin), removing the dipeptide threonyl-asparagine (Thr147-Asn148).[51] However, the minor component and its corresponding acyl-enzyme derivatives were not observed in the present study.

As seen from Figure 3.1, the chymotrypsin component is accompanied by satellite peaks centered at 25,430 (M-19) and 25,472 (M+23), while the pMC-CHT component is accompanied by satellite peaks centered at 25,592 (M-18), 25,632 (M+22), 25655 (M+45), and 25674 (M+64). Satellite peaks at masses higher than the base peak often result from the formation of sodium adduct ions, where a charge center normally occupied by an additional proton is instead occupied by a sodium ion. The mass difference between these satellite peaks and the base peak are integer multiples of 22, the difference in nominal mass between sodium and hydrogen. Even though many of the satellite peaks are not centered at exact multiples of 22, they have peak widths on the order of 15-20 Da, thus they can be positively attributed to sodium adduct ions. The

additional, poorly resolved peaks beyond the sodium adduct peaks are likely protein impurities, though they are not identified at this time.

The satellite peaks found with a lower mass than the identified base peaks for both pMC-CHT and free chymotrypsin cannot be identified as sodium adducts, as the base peaks already correspond to the theoretical masses of the free enzyme and the acyl-enzyme intermediate. In addition, they are not deconvolution artifacts as the corresponding peaks can be found in the original mass spectrum. Instead, the 25,430 Da peak (M-19) is most likely due to the presence of another chymotrypsin isoform, δ-chymotrypsin, with a theoretical molecular mass of 25,430.9 Da, as it has been demonstrated previously that multiple isoforms are commonly found in commercial preparations of α-chymotrypsin.[50] The monosodium adduct of δ-chymotrypsin would therefore appear at 25,452 Da, overlapping with the α_1-chymotrypsin base peak. This accounts for the unusual peak height patterns observed here, where the highest peak is located at an intermediate mass, instead of being at the lowest mass, as in the case of a single protein with its sodium adducts. Similarly, the 25,592 Da peak (M-18) is identified as the corresponding acyl-enzyme of δ-chymotrypsin. These satellite features are also observed in the mass spectra of the other acyl-enzymes.

As in the case of α_1-chymotrypsin, δ-chymotrypsin also has the peptide bond between amino acids 148-149 intact, thus containing the activation dipeptide Thr147-Asn148. The two differ in that Thr147 is also bonded to Tyr146 in δ-chymotrypsin, whereas in α_1-chymotrypsin that peptide bond is hydrolyzed. The addition of H_2O during hydrolysis accounts for the nominal mass difference of 18 Da between the two isoforms.

The presence of α_1-chymotrypsin and δ-chymotrypsin instead of α-chymotrypsin does not affect the conclusion of the present study. They differ from α-chymotrypsin only in the hydrolysis of two peptide bonds during activation from chymotrypsinogen A, and the presence of the activation dipeptide Thr147-Asn148 does not markedly alter the overall properties of the protein,[52] nor does it eliminate the catalytic activity of the enzyme.[49, 50] More importantly, the goal of the present work is to study the hydrogen bonding interaction between different inhibitors and the oxyanion hole of chymotrypsin, and, as the same isoforms are used across the four inhibitors, the reported results should be considered general.

3.2 Kinetics Measurements

The chymotrypsin-catalyzed hydrolysis follows this general reaction scheme:

$$E + S \underset{k_{-1}}{\overset{k_1}{\leftrightarrow}} ES \overset{k_2}{\rightarrow} EP_2 + P_1 \overset{k_3}{\rightarrow} E + P_2 \quad (3)$$

For the hydrolysis of esters and imidazoles, formation of ES (k_1) and the acyl-enzyme intermediate EP_2 (k_2) occurs rapidly. The deacylation reaction (k_3) is the rate-limiting step,[45, 53] and the reaction follows first-order kinetics, with the rate law as follows:

$$\frac{d[P_2]}{dt} = k_3[EP_2] \quad (4)$$

As we expect the strength of the interaction between the inhibitor and the oxyanion hole in the acyl-enzyme intermediate to be reflected in the hydrolysis rate, we measured k_3 using a chymotrypsin activity assay and direct UV-visible observation of the acyl-enzyme intermediate.

3.2.1 Chymotrypsin Activity Assay

When an inhibitor acylates chymotrypsin, the resultant acyl-enzyme intermediate is catalytically inactive and cannot hydrolyze additional substrate. Once the acyl-enzyme hydrolyzes, the free enzyme is released and activity returns. Therefore, k_3 can be determined by measuring the rate at which chymotrypsin activity returns. The operational normality of chymotrypsin is measured by tracking the hydrolysis of N-benzoyl-L-tyrosine ethyl ester (BTEE) in the enzyme solution over a period of 3 minutes, with a standard solution of free, uninhibited chymotrypsin as a control sample against which the acyl-enzyme samples are compared. As the reported hydrolysis rates for oMC-CHT and

pMC-CHT were high enough to lower the concentration of acyl-enzyme over the measurement period, this method is only feasible for DAB-CHT.

Figure 3.2 shows a plot of ln(percentage enzyme activity) over time. As the deacylation reaction follows first-order kinetics, the slope of the line corresponds to k_3, and for DAB-CHT it was determined to be $6.0 \pm 0.7 \times 10^{-6}$ s^{-1}.

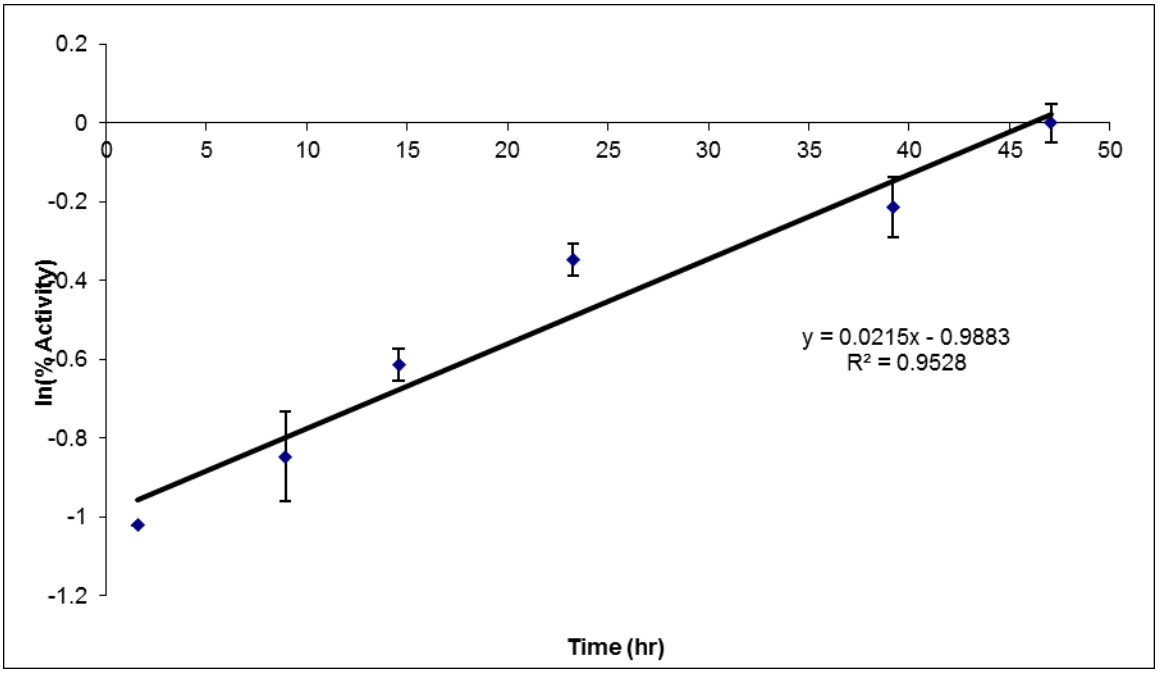

Figure 3.2: Chymotrypsin activity assay of DAB-CHT. The degree of hydrolysis was determined via the activity of the acyl-enzyme solution against a control solution of α-chymotrypsin. As the acyl-enzyme hydrolyzes, the activity returns. Hydrolysis rate constant (k_3) is calculated using the slope from linear regression ($r^2 = 0.9528$, n = 3).

The calculated rate constant is in rough agreement with the previously reported value[53] of $1 \pm 1 \times 10^{-6}$ s^{-1}, measured via UV-visible spectroscopy. Although both studies used similar hydrolysis conditions, the addition of 53 mM $CaCl_2$ in the present study in accordance to the Sigma-Aldrich protocol[46] is likely responsible for the higher observed

rate constant. α-chymotrypsin is known to exhibit increased activity in the presence of calcium ions.[54]

It was also noted in Figure 3.2 that some points in the plot deviate from linearity. With chymotrypsin being a proteolytic enzyme, self-digestion is possible and could account for the variability of measurements. Though the hydrolysis of the acyl-enzyme complex follows first-order kinetics, the autolysis of the enzyme follows a complex kinetic profile, and may follow second-order kinetics.[55] The different concentrations in catalytically active chymotrypsin in the acyl-enzyme samples and the control will therefore lead to different autolysis rates. Thus, enzyme activity as a measure of concentration of covalently bonded acyl-enzyme complex may be confounded.

3.2.2 UV-Vis Spectroscopy

As both benzoyl and cinnamoyl derivatives absorb strongly in the ultraviolet region, UV-vis spectroscopy was used to directly measure the presence of acyl-chymotrypsin intermediates DAB-CHT, oMC-CHT, and pMC-CHT, as was demonstrated previously.[53, 56, 57] Since this method does not require tracking the concentration of hydrolysis products over time, it is more suitable for characterization of acyl-enzymes with short half-lives.

As seen in Figure 3.3 for DAB-CHT, there is a distinctive acyl-enzyme peak at 327 nm that decreases as the acyl-enzyme hydrolyzes. There is also a corresponding time-dependent increase in the 250 nm to 305 nm range that is attributed to the deacylation product, *p*-N,N-dimethylaminobenzoic acid, although the magnitude of the change is smaller than the 327 nm peak and there is significant overlap with the broad enzyme absorption peak centered at 280 nm.

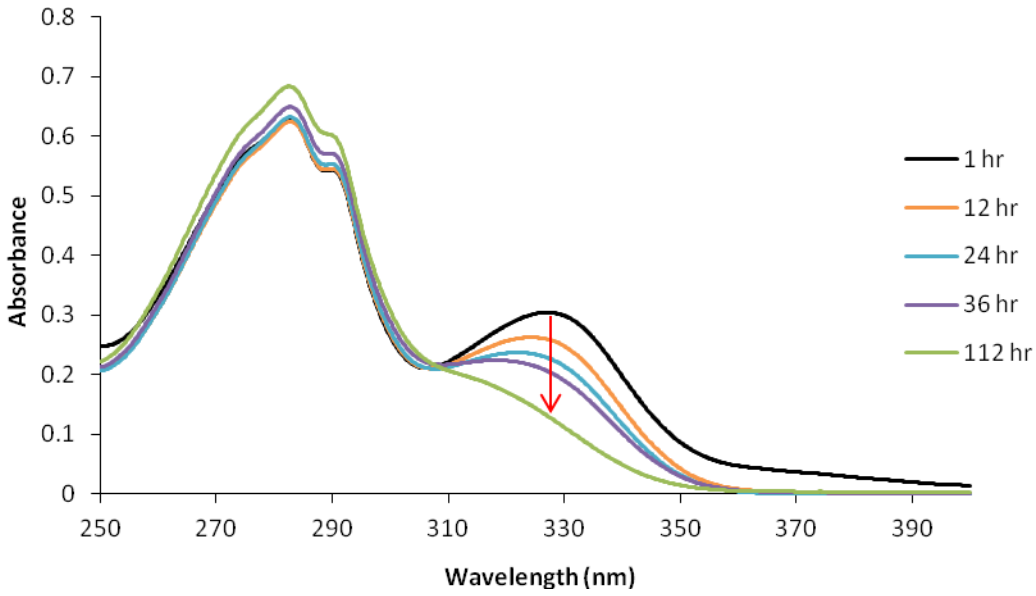

Figure 3.3: UV-Vis spectra of *p*-N,N-dimethylaminobenzoyl-α-chymotrypsin (DAB-CHT) at 1, 12, 24, 36, and 112 hours after the initial formation of the acyl-enzyme. The acyl-enzyme peak at 327 nm (noted with a red arrow) decreases as a function of time.

The difference spectra for the three acyl-enzymes are shown in Figure 3.4 to Figure 3.6. Like DAB-CHT, oMC-CHT and pMC-CHT also show similar absorption peaks near 345 nm that decreases as a function of time, corresponding to the hydrolysis of the acyl-enzyme complexes. The free acids for these two acyl-enzymes also absorbs at lower wavelengths, at about 260 nm and 310 nm for oMC, and 290 nm for pMC. As tracking the decrease in absorbance at the higher wavelengths of 330-350 nm range yielded the best linear fit in a semi-log plot for the three acyl-enzymes, those peaks were used to determine k_3.

The difference spectrum for DAB-CHT also reveals increases in absorbance at 281.7 nm and 288.9 nm, most evident at the 112 hr time point as two small peaks. These

features were noted previously by Bender *et al*,[56] and are attributed to the differences in absorbance of acyl-chymotrypsin and free chymotrypsin.

Other features in the difference spectra could also be used to comment on the extent of the reaction and presence of any side reactions. For a given reaction, one would expect the concentration of a reactant to decrease while that of the product to increase, therefore the difference spectrum should reflect changing absorbances at various wavelengths. At certain wavelengths, however, the molar absorptivities are the same for the reactant and the product, and the absorbance at those wavelengths does not change as the reaction progresses. These are identified on the difference spectrum as isosbestic points where the lines intersect. These are ideal reference points as any deviations from the isosbestic point indicate the presence of additional species, or other sources of error such as instrument variability.

For DAB-CHT, the isosbestic point is located at around 309 nm, and there are no significant deviations until the 112 hour time point. Given the significant period of time for side reactions to occur, this is not surprising as autolysis and other conformational changes are known to lead to noticeable changes in optical properties.[51] The difference spectra for oMC-CHT and pMC-CHT show no obvious deviations in the isosbestic points, save for the 99 minute time point for oMC-CHT, which does not intersect at 281 nm. However, as shown later this does not appear to impact the absorbance changes at the wavelengths of interest. Overall, the isosbestic points in the difference spectra suggest that the species involved in the desired acyl-enzyme hydrolysis is dominantly responsible for the spectroscopic changes observed here.

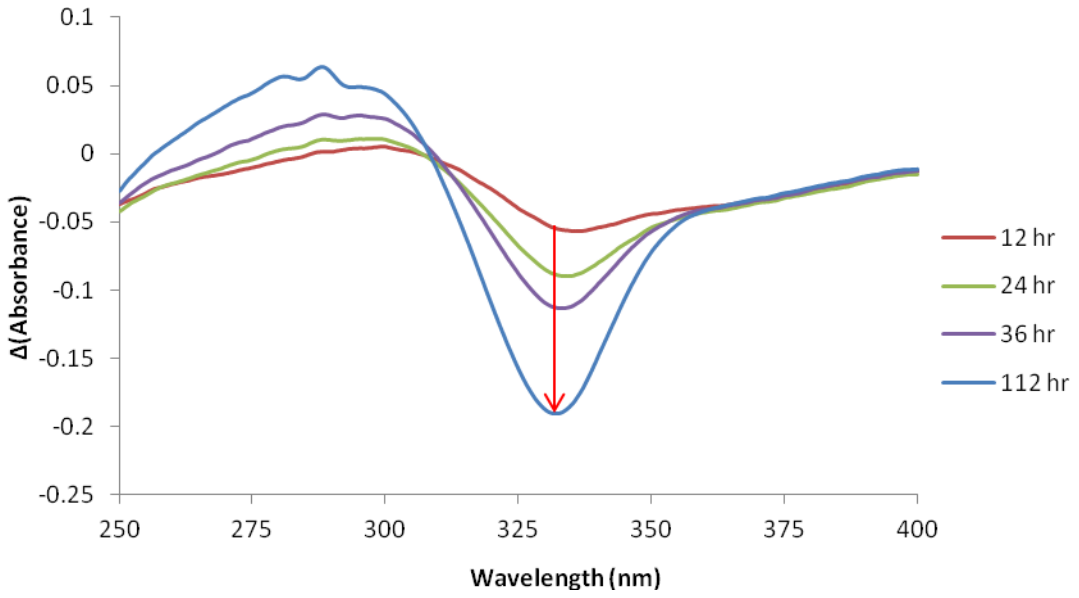

Figure 3.4: Difference UV-Vis Spectrum for DAB-CHT at 12, 24, 36, and 112 hours after the initial formation of the acyl-enzyme.

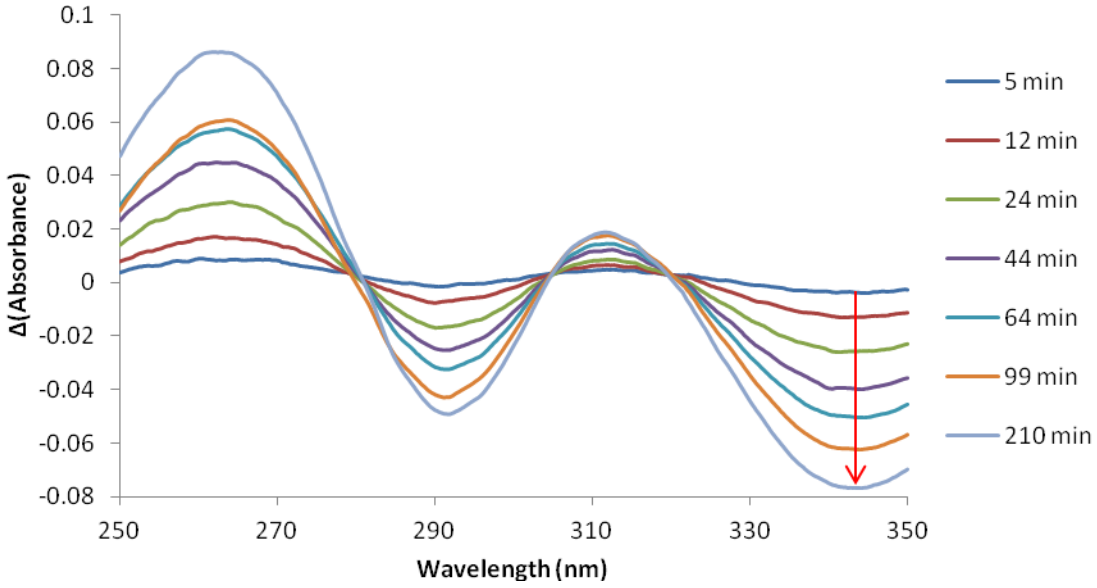

Figure 3.5: Difference UV-Vis Spectrum for oMC-CHT at 5, 12, 24, 44, 64, 99 and 210 minutes after the initial formation of the acyl-enzyme.

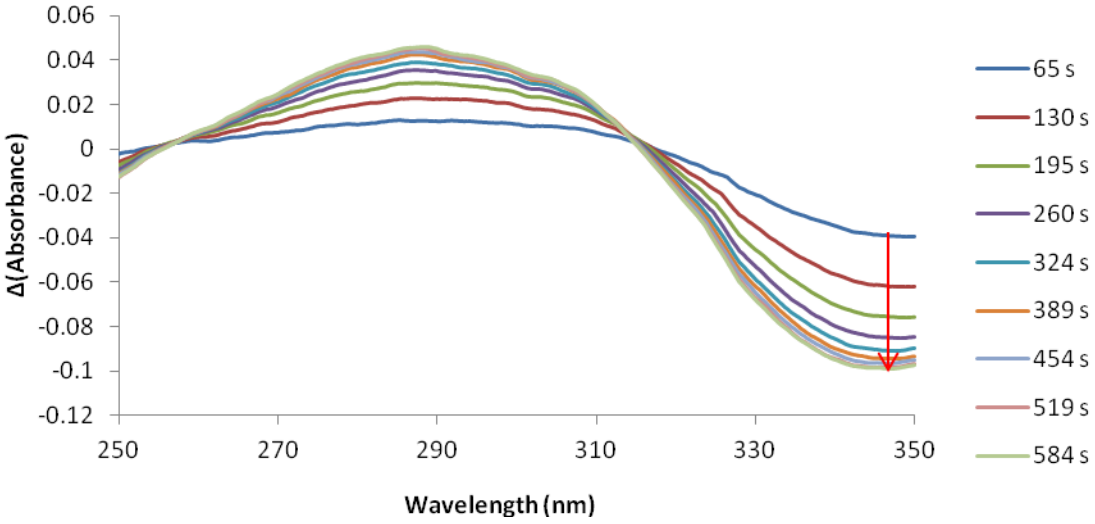

Figure 3.6: Difference UV-Vis Spectrum for pMC-CHT at 65, 130, 195, 260, 324, 389, 454, 519 and 584 seconds after the initial formation of the acyl-enzyme.

The hydrolysis rate constant (k_3) for DAB-CHT, oMC-CHT, and pMC-CHT were determined by plotting ln(A) at 327.0, 343.7, and 348.9 nm, respectively, against time (Figure 3.7 to Figure 3.9). The three plots display a high degree of linearity, all with a linear regression coefficient r^2 greater than 0.99.

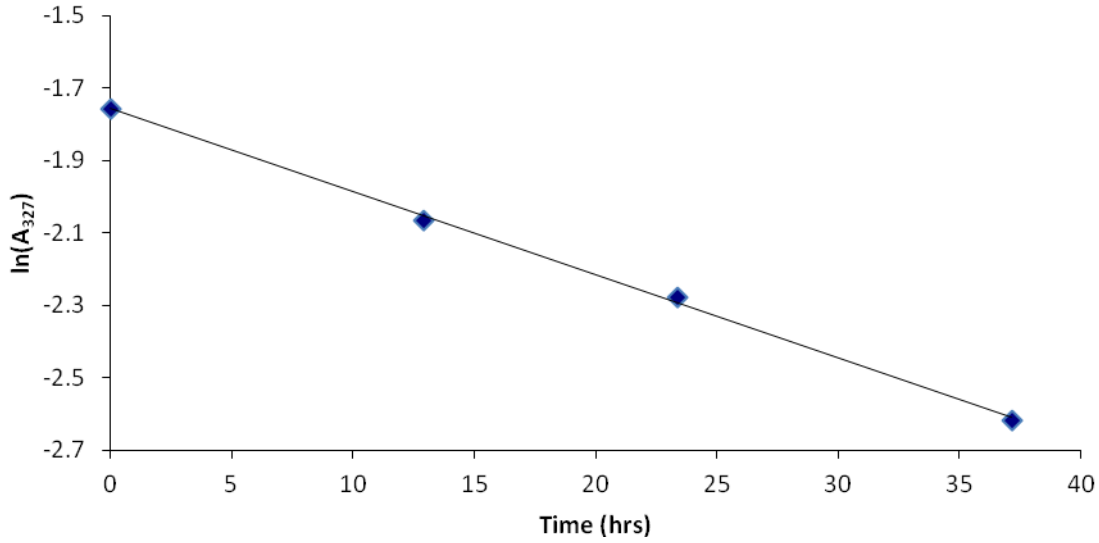

Figure 3.7: Hydrolysis of DAB-CHT, determined by tracking absorbance at 327 nm. Hydrolysis rate constant (k_3) is calculated using the slope from linear regression (r^2 = 0.9990).

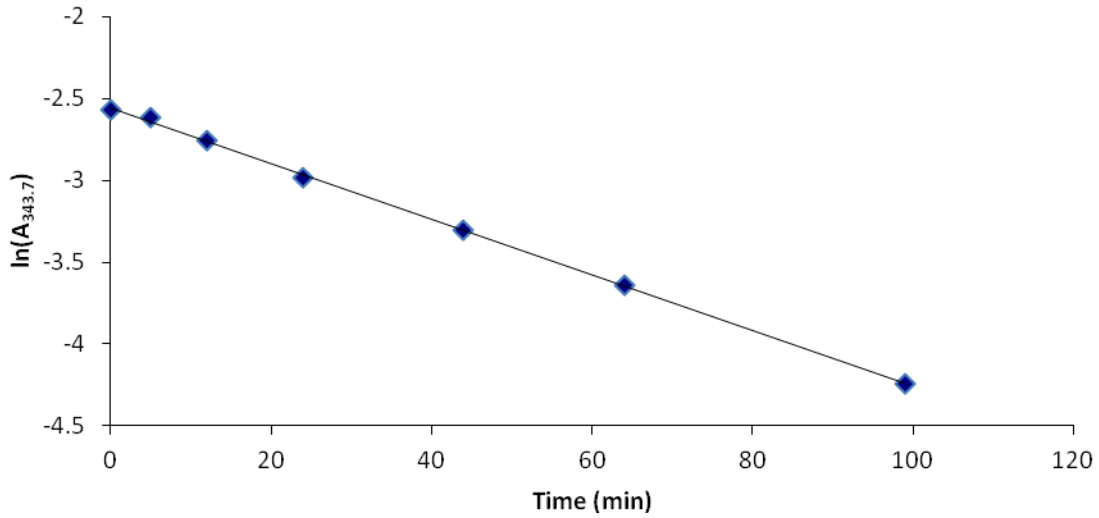

Figure 3.8: Hydrolysis of oMC-CHT, determined by tracking absorbance at 343.7 nm. Hydrolysis rate constant (k_3) is calculated using the slope from linear regression (r^2 = 0.9996).

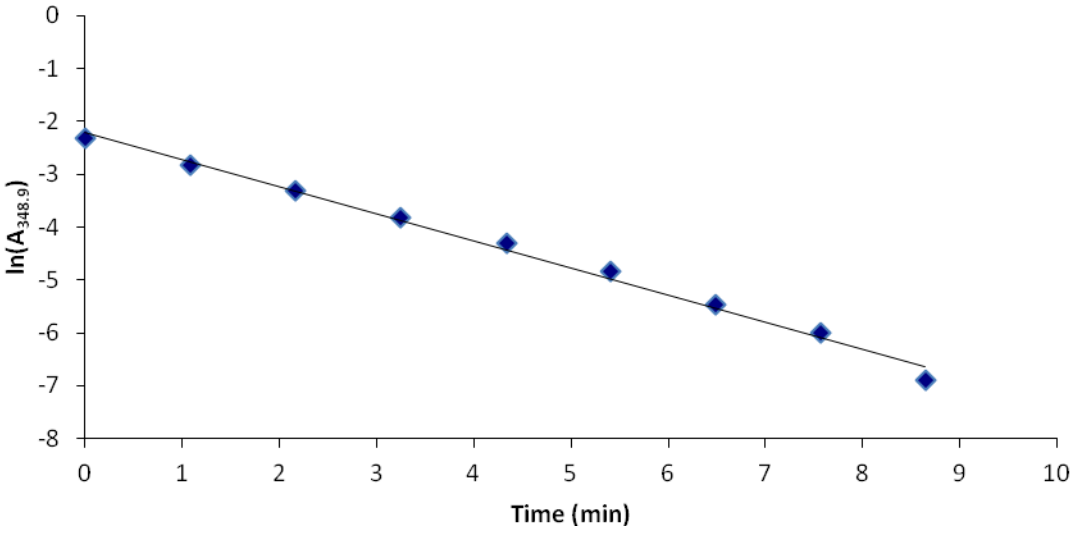

Figure 3.9: Hydrolysis of pMC-CHT, determined by tracking absorbance at 348.9 nm. Hydrolysis rate constant (k_3) is calculated using the slope from linear regression (r^2 = 0.9927).

The experimental rate constants determined by the UV-vis method are summarized in Table 3.2. The relative hydrolysis rates of the acyl-enzymes were determined to be pMC-CHT > oMC-CHT > DAB-CHT. With the UV-vis method, the deacylation rate for DAB-CHT was $6.4 \pm 0.1 \times 10^{-6}$ s^{-1}, which is consistent with the one obtained in the previous section via chymotrypsin activity assay, $6.0 \pm 0.7 \times 10^{-6}$ s^{-1}.

Table 3.2: Hydrolysis rate constants for selected acyl-enzyme intermediates, as measured via UV-vis spectroscopy.

Acyl-Enzyme Intermediate	Deacylation Rate, k_3 (s^{-1})	
	Literature values	Experimental
DAB-CHT	$1 \pm 1 \times 10^{-6}$ [a]	$6.4 \pm 0.1 \times 10^{-6}$
oMC-CHT	1.9×10^{-4} [b]	$2.8 \pm 0.1 \times 10^{-4}$
pMC-CHT	2.52×10^{-3} [b]	$8.5 \pm 0.3 \times 10^{-3}$

[a] Measured rate of hydrolysis in pH 7.8 phosphate buffer.[53]

[b] Calculated with reported formula using maximum rate of hydrolysis for pH 7.8. Error bounds were not reported.[58]

The measured rate constants for all three acyl-enzyme intermediates are in general agreement with reported literature values.[53, 58] However, it is noted that all our measured rate constants are somewhat higher than the literature values, and this could be due to the aforementioned differences in $CaCl_2$ concentrations.

This series of kinetic measurements have firmly established the conditions central to our objective. As the oxygen atom is central in the interaction between the oxyanion hole and the scissile carbonyl group, its ^{17}O NMR parameters should reflect any key intermolecular interactions that give rise to these observed kinetic differences.

3.3 Solid-State ^{17}O NMR Spectra of Acyl-Enzyme Intermediates

Once the integrity of the acyl-enzymes were established by mass spectrometry and the kinetics of acyl-enzyme hydrolysis was determined by UV-vis, we obtained solid-state ^{17}O-NMR spectra for DAB-CHT, oMC-CHT, and pMC-CHT. As shown in Figure 3.10, each ^{17}O MAS NMR spectrum exhibits a central signal with two weak spinning sidebands.

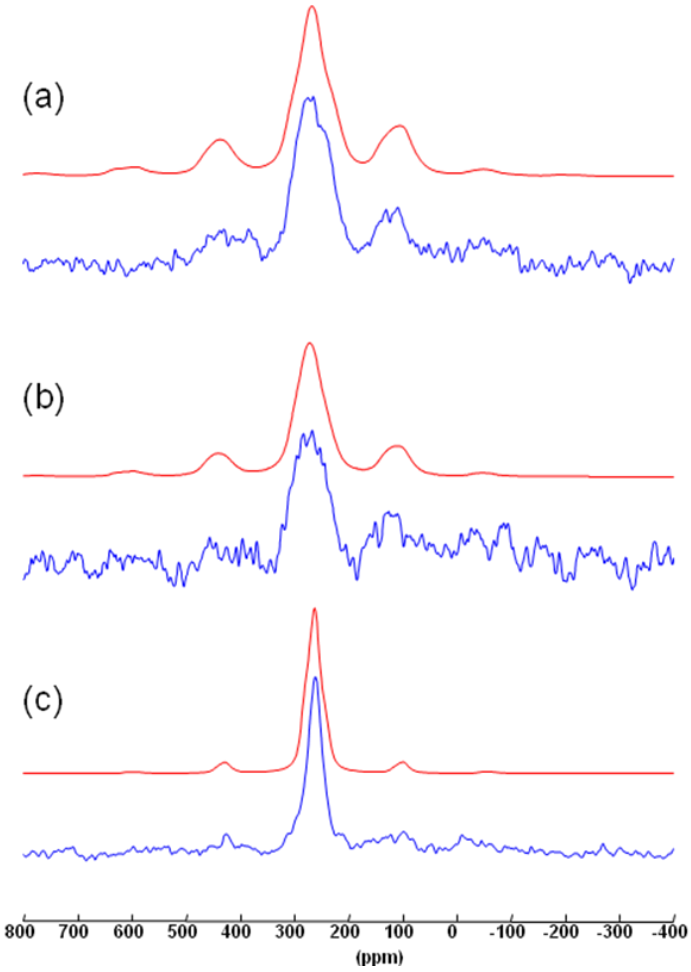

Figure 3.10: Experimental spectra (blue) and computed spectra (red) for the 3 acyl-enzyme intermediates: a) DAB-CHT, b) oMC-CHT, c) pMC-CHT. The sample was prepared by packing 20 mg acyl-enzyme into a 3.2 mm ZrO_2 rotor. The experimental spectra were obtained at 21.1 T under MAS conditions, with a spin rate of 20 kHz and recycle delay of 30 ms. The number of transients were: a) 2.0×10^6 b) 2.2×10^6 c) 1.5×10^6.

The isotropic chemical shift (δ_{iso}), chemical shift tensor components (δ_{11}, δ_{22}, δ_{33}), quadrupolar coupling constant (C_Q), asymmetry parameter (η_Q) were obtained from the spectral analysis. δ_{iso}, C_Q, and η_Q were directly obtained as they are input parameters in calculating the theoretical spectra, while the CS tensor components were calculated from other input parameters, chemical shift anisotropy (δ_{CS}) and asymmetry (η_{CS}), using the following relations:

$$\delta_{CS} = \delta_{33} - \delta_{iso} \quad (4)$$

$$\eta_{CS} = (\delta_{22} - \delta_{11})/\delta_{CS} \quad (5)$$

As those two parameters are estimated with less precision, the calculated tensor components have greater uncertainty. The ^{17}O NMR parameters are summarized in Table 3.3.

Table 3.3: Experimental ^{17}O NMR parameters for the three acyl-enzyme intermediates.

Acyl-enzyme	δ_{iso} (ppm)	δ_{11} (ppm)	δ_{22} (ppm)	δ_{33} (ppm)	C_Q (MHz)	η_Q
DAB-CHT	316 ± 2	614 ± 10	369 ± 10	-34 ± 10	10.0 ± 1	0.6 ± 0.2
oMC-CHT	310 ± 2	565 ± 10	355 ± 10	10 ± 10	9.2 ± 1	0.6 ± 0.2
pMC-CHT	288 ± 2	458 ± 10	318 ± 10	88 ± 10	7.0 ± 0.5	0.8 ± 0.2

The isotropic chemical shifts (δ_{iso}), two chemical shift tensor components (δ_{11} and δ_{22}) and the quadrupolar coupling constants (C_Q) follow the same trend in the three inhibitors studied: DAB-CHT > oMC-CHT > pMC-CHT. The asymmetry parameter (η_Q) and the third chemical shift tensor component, δ_{33}, on the other hand, follow the opposite trend. Previous ^{17}O NQR studies on hydrogen-bonded formaldehyde[16] and other organic molecules[17] reported that the ^{17}O nuclear quadrupolar coupling constant decreases with increasing hydrogen bonding strength. Likewise, experimental ^{17}O NMR studies of

peptides[10] and small-molecule amides[12, 15], as well as computational studies,[11, 15, 18, 59] have shown the same trend for both δ_{iso} and C_Q.

It has been demonstrated via Raman spectroscopic studies of acyl-chymotrypsin complexes[44] that a stronger hydrogen-bonding environment in the oxyanion hole provides greater transition state stabilization, leading to a higher deacylation rate of the acyl-enzyme. Therefore, pMC-CHT, having the highest deacylation rate constant, would have the strongest hydrogen bond interactions in the oxyanion hole. The trends in the observed NMR parameters support the kinetic data and the hydrogen bond environments of each acyl-chymotrypsin complex. The chemical shift anisotropy (defined as the span $\Omega = \delta_{11} - \delta_{33}$) displays an even greater sensitivity toward hydrogen bonding than does δ_{iso}: DAB-CHT (648 ppm) > oMC-CHT (555 ppm) > pMC-CHT (370 ppm). This is because δ_{11} and δ_{33} change in the opposite directions to respond to hydrogen bonding. As the changes in δ_{11} and δ_{33} are of opposite signs, the resultant change to δ_{iso} is attenuated. The trends in these ^{17}O NMR parameters for the acyl-enzymes are in agreement with those previously observed for small molecules.[12, 15] It is important to note that the principal tensor components can only be obtained via solid-state NMR experiments, as in the liquid state the chemical shift components are averaged to the isotropic value.

3.4 Computational Results

The current study thus far discussed experimentally derived ^{17}O NMR parameters in the context of hydrogen bond strength as established by hydrolysis rates of various acyl-enzyme intermediates. However, the strength of hydrogen bonding is determined by a number of structural factors, including hydrogen bond distances and general geometry of atoms involved in the hydrogen bond. In a theoretical MO study on hydrogen-bonded peptides, Kuroki *et al*[11] reported that ^{17}O NMR chemical shift, quadrupolar coupling constant, and asymmetry parameter changes as a function of the hydrogen bond length, bond angle, and dihedral angle. We must therefore consider the effects of these factors when discussing the origins of the observed ^{17}O NMR parameters.

Using a similar computational approach, we examined the relationship between calculated NMR parameters and hydrogen bond distance, bond angle, and dihedral angles. A series of density functional theory computations using *Gaussian 09* were performed on various model compounds.

3.4.1 Electronic Effects of the Aryl Substituent

To examine how ^{17}O NMR parameters depend on the nature of the aryl substituent (Figure 2.1), rather than differences in hydrogen bonding at the oxyanion hole, we first computed ^{17}O NMR parameters for isolated (hydrogen-bond free) inhibitor models. Since the key covalent bond in the acyl-enzyme is an ester bond between the carbonyl group of the substrate and the serine-195 hydroxyl functional group from the enzyme, we constructed simple ethyl ester analogues for this part of the study. This eliminates any non-covalent interactions between the enzyme and the inhibitor, while

retaining the ester functional group. The computed ^{17}O NMR parameters for the ethyl esters analogues are summarized in Table 3.4.

Table 3.4: Calculated ^{17}O NMR parameters for isolated ethyl ester inhibitor analogues.

Ethyl ester analogue	δ_{iso} (ppm)	δ_{11} (ppm)	δ_{22} (ppm)	δ_{33} (ppm)	C_Q (MHz)	η_Q
DAB-Et	329.1	576.5	463.4	-52.8	8.44	0.0
oMC-Et	330.1	574.3	472.4	-56.3	8.32	0.0
pMC-Et	326.1	569.0	467.3	-58.0	8.27	0.0

It is seen immediately from Table 3.4 that all three compounds exhibit very similar ^{17}O NMR parameters. In addition, the calculated δ_{iso}, C_Q, and η_Q are markedly different than the experimentally obtained values in Table 3.3. This is expected, as these calculations are done in the absence of any hydrogen bonds. More importantly, the set of calculated chemical shifts and quadrupolar coupling constants for the three ethyl ester analogues show much less variation than the experimentally obtained values for the acyl-enzymes. While the acyl-enzymes exhibit δ_{iso} that cover a range of almost 30 ppm and C_Q that covers a range of 3 MHz, the respective NMR parameters for the isolated ethyl esters only cover 4 ppm and 0.2 MHz. Comparing the calculated chemical shift tensor components of the ethyl esters to that of the acyl-enzymes reveals a starker contrast: between the three ethyl ester models, δ_{11}, δ_{22} and δ_{33} only span a range of about 7 ppm, 5 ppm, and 6 ppm, respectively, while the experimentally measured parameters of the acyl-enzymes covers a range of 150 ppm, 50 ppm, and 110 ppm, respectively. In addition, in the acyl-enzymes, δ_{33} has a trend opposite to δ_{11} and δ_{22} – a characteristic of changes in hydrogen-bonding environment – but this trend is absent in the ethyl ester analogues.

We therefore conclude that the differences we observed in experimental NMR parameters in the acyl-enzymes are due to more complex intermolecular actions with the enzyme, rather than electronic effects arising from the aryl substituents.

3.4.2 Effect of the Hydrogen Bond Length

To gain a more complete understanding of the relationship between ^{17}O NMR parameters and structural features in acyl-enzyme complexes, we next examined the effect of hydrogen bond length on the ^{17}O NMR parameters using a simple model where two N-methylacetamide molecules form two hydrogen bonds to the ethyl-ester analogues of the acyl-enzyme intermediates. Here we adopted a similar geometry as used by de Dios and Oldfield in their study of carbonyl ^{13}C chemical shifts in peptides.[13] As seen from Figure 3.11, the model mimics the hydrogen bond interaction seen in the oxyanion hole of serine proteases. An ideal hydrogen bond configuration is adopted with the C=O···H hydrogen bond angles set at 120°, while the proton lies in the $O_1=C_1-O^{\gamma}$ plane to maximize the interaction with lone pair electrons residing in sp^2-hybridized orbitals of the carbonyl oxygen.[60] Instead of positioning the hydrogen bond donor and acceptor molecules on the same plane, the two N-methylacetamide molecules are set orthogonal to the $O_1=C_1-O^{\gamma}$ plane in an anti-parallel configuration to mimic the backbone of Ser195 and Gly193 which forms the oxyanion hole of α-chymotrypsin (see Figure 3.16). The two N···O hydrogen bond distances were set to be equal, and varied systematically from a short HB length (2.5 Å) to a moderate HB length (3.2 Å). For each HB length, ^{17}O NMR parameters were computed. The results of the computation are illustrated in Figure 3.12.

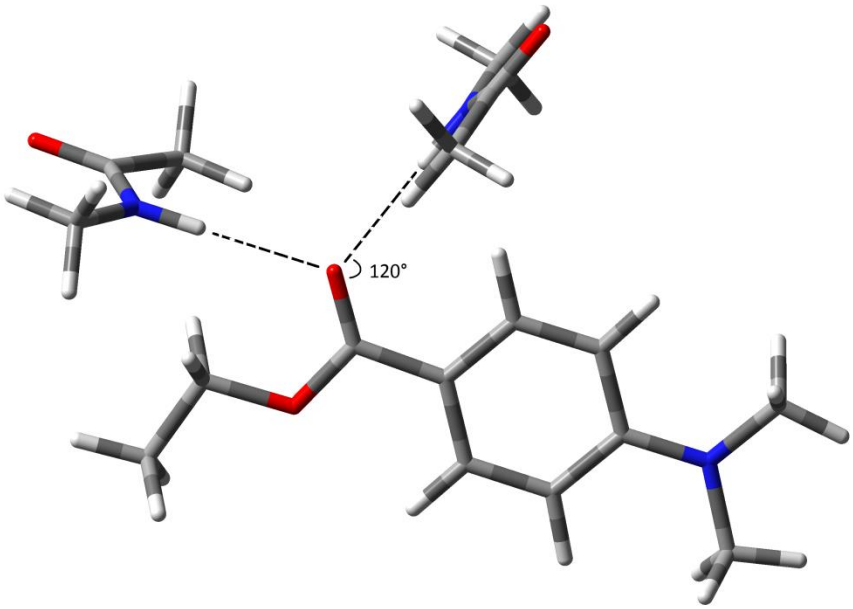

Figure 3.11: Hydrogen bond model with ethyl *p*-N,N-dimethylaminobenzoate (DAB-Et). The protein backbone hydrogen bond donors of the oxyanion hole of acyl-chymotrypsin are simulated with two N-methylacetamide molecules.

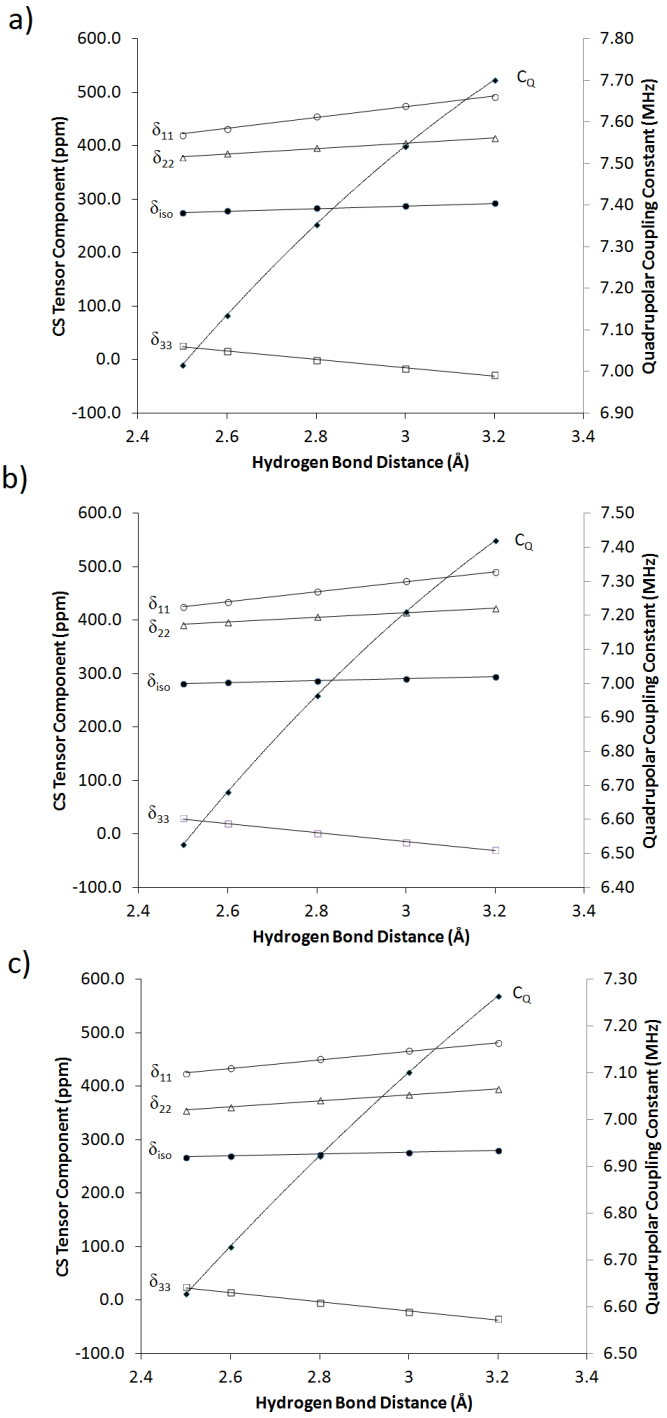

Figure 3.12: Chemical shift tensor components, isotropic chemical shift, and quadrupolar coupling constant as a function of hydrogen bond distance of a) DAB-Et, b) oMC-Et, c) pMC-Et, as a function of hydrogen bond distance in our model of the oxyanion hole. The protein backbone hydrogen bond donors of the oxyanion hole of acyl-chymotrypsin are simulated with N-methylacetamide.

As seen from Figure 3.12, the three hydrogen-bonded ethyl ester analogues exhibit essentially the same trends in the ^{17}O NMR parameters as a function of the hydrogen bond length. As the hydrogen bond distance decreases, δ_{11} and δ_{22} decrease while δ_{33} increases, consistent with the established trends.[12, 15] For DAB-Et, oMC-Et and pMC-Et in the presence of hydrogen bonds of a moderate length ($r_{N\cdots O}$ = 3.2 Å), the computed isotropic ^{17}O chemical shifts were 292.2, 294.1, and 280.0 ppm, respectively, compared to 329.1, 330.1, and 326.1 ppm, for the corresponding free ethyl ester analogues (see Table 3.4). The ^{17}O quadrupolar coupling constant, C_Q, also decreases as a function of the hydrogen bond distance for all three models. While the isolated ethyl ester analogues exhibit similar C_Q of 8.44, 8.32, and 8.27 MHz for DAB-Et, oMC-Et, and pMC-Et, respectively, the C_Q values were lowered to 7.70, 7.42, and 7.26 MHz when the hydrogen bond distance was 3.2 Å. Though the relationship between C_Q with hydrogen bond distance has been documented in both computational[16] and experimental[17] studies, the change we observed here is much smaller than the range in C_Q exhibited in our experimental data where C_Q for DAB-CHT, oMC-CHT, and pMC-CHT are 10.0 MHz, 9.2 MHz, and 7.0 MHz, respectively (Table 3.4), having a range of 3 MHz between the acyl-enzymes.

Over the range of hydrogen bond distances examined, δ_{iso} for DAB-Et, oMC-Et and pMC-Et span 17.4, 12.4, and 12.2 ppm, respectively. These variations are significantly larger than changes due to the electronic effect of aryl substituents examined in the previous section. However, examining the isotropic value alone may be misleading. In fact, the individual tensor components demonstrate a much higher

sensitivity. For example, at the hydrogen bond distances examined, the tensor components δ_{11}, δ_{22}, and δ_{33} for DAB-Et span 72, 36, and 55 ppm, respectively. Changes in the isotropic chemical shift appear attenuated only because δ_{11} and δ_{22} follow the opposite trend to δ_{33}.

By comparison, the ^{13}C chemical shift tensor of the carbonyl carbon in the same model shows a lower sensitivity, as seen from Figure 3.13. As the hydrogen bond distance decreases for DAB-Et, δ_{iso} only increases by 3 ppm, while δ_{11} decreases by 12 ppm and δ_{22} increases by 25 ppm. δ_{33} is relatively insensitive, only decreasing by 5 ppm. Other studies on carbonyl carbons in hydrogen-bonded systems showed similar sensitivity: over the same hydrogen bond distances examined (2.5 Å – 3.2 Å), δ_{iso} was found to change by 15 ppm[61] and 9 ppm[62] for solid-state L-alanine and L-glycine, respectively. The opposing trends between δ_{11} and δ_{22}, as well as the lack of sensitivity of δ_{33}, were also seen in those studies.

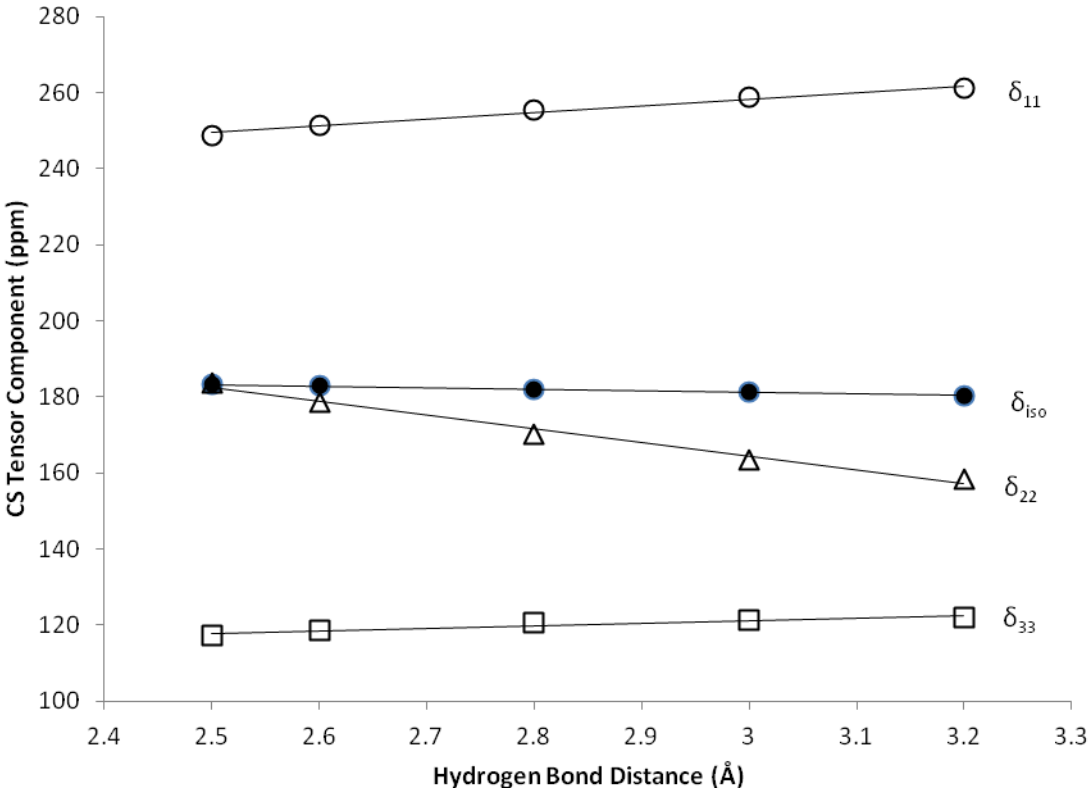

Figure 3.13: ^{13}C isotropic chemical shift and chemical shift tensor components as a function of hydrogen bond distance.

3.4.3 Effect of Hydrogen Bond Direction

In the previous section, we examined the effect of ^{17}O NMR parameters as a function of the O···N length. It is well known that the direction of hydrogen bonds can affect hydrogen bond strength as well, so their effect on NMR parameters was also examined. As outlined in a survey of enzymes containing oxyanion holes and small molecule analogues of oxyanion holes by Simón and Goodman,[63] enzymes often contain hydrogen bonds that deviate from an arrangement that allows for ideal interactions. Specifically, the X···O=C-R dihedral angle Θ (Figure 3.14), where X is the heteroatom of the hydrogen bond donor, is frequently found to be at near 90° in enzymes. One would expect the optimal dihedral angle to be 0°, as commonly seen in the crystal structures of small molecules,[60, 63] since in that configuration the protons lie in the same plane as the lone pair electrons in sp^2 hybridized orbitals of the carbonyl oxygen. The suboptimal arrangement is theorized to allow for stabilization of the transition state without stabilizing the ground state reactant, which would hinder the catalysis provided by the enzyme.[63]

We sought to elucidate the effect of hydrogen bond angle on the inhibitor model. Accordingly, we fixed the hydrogen bond distance at 2.5 Å in our hydrogen bond model while varying the X···O=C-R dihedral angle concurrently from 0° (Figure 3.11) to 90° (Figure 3.14) at 10° increments.

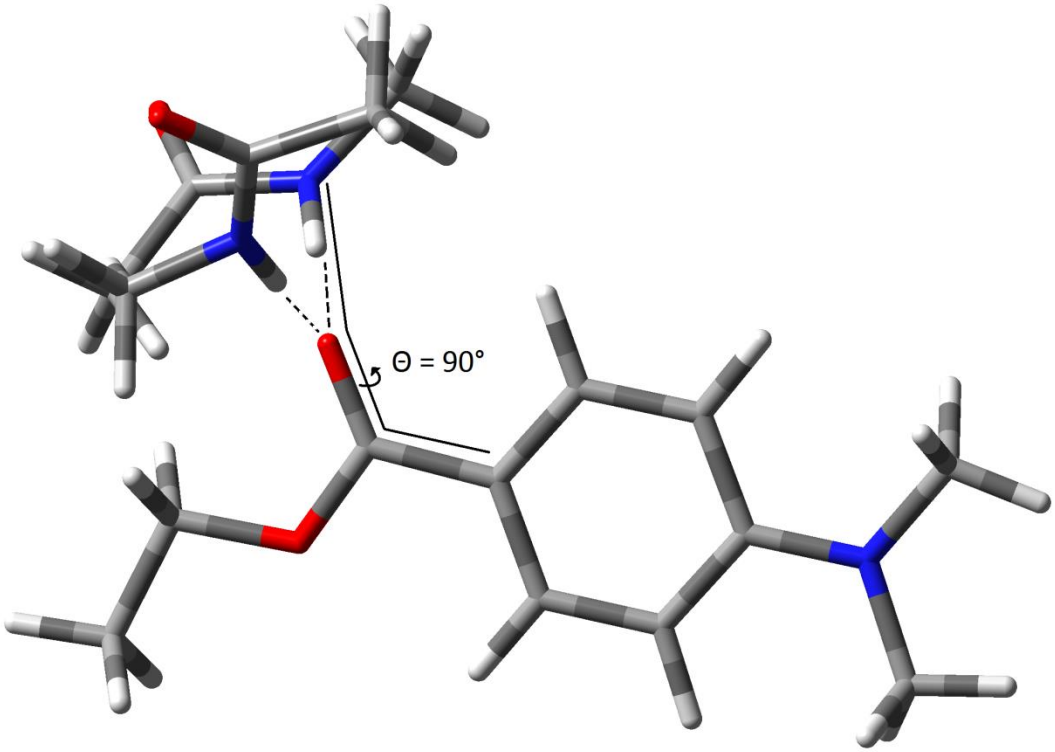

Figure 3.14: Hydrogen bond model with ethyl *p*-N,N-dimethylaminobenzoate (DAB-Et), with the N···O=C-R dihedral angle, Θ, at 90°.

The relationship between the ^{17}O chemical shift tensor components, quadrupolar coupling constant, and the N···O=C-R dihedral angle, Θ, can be found in Figure 3.15.

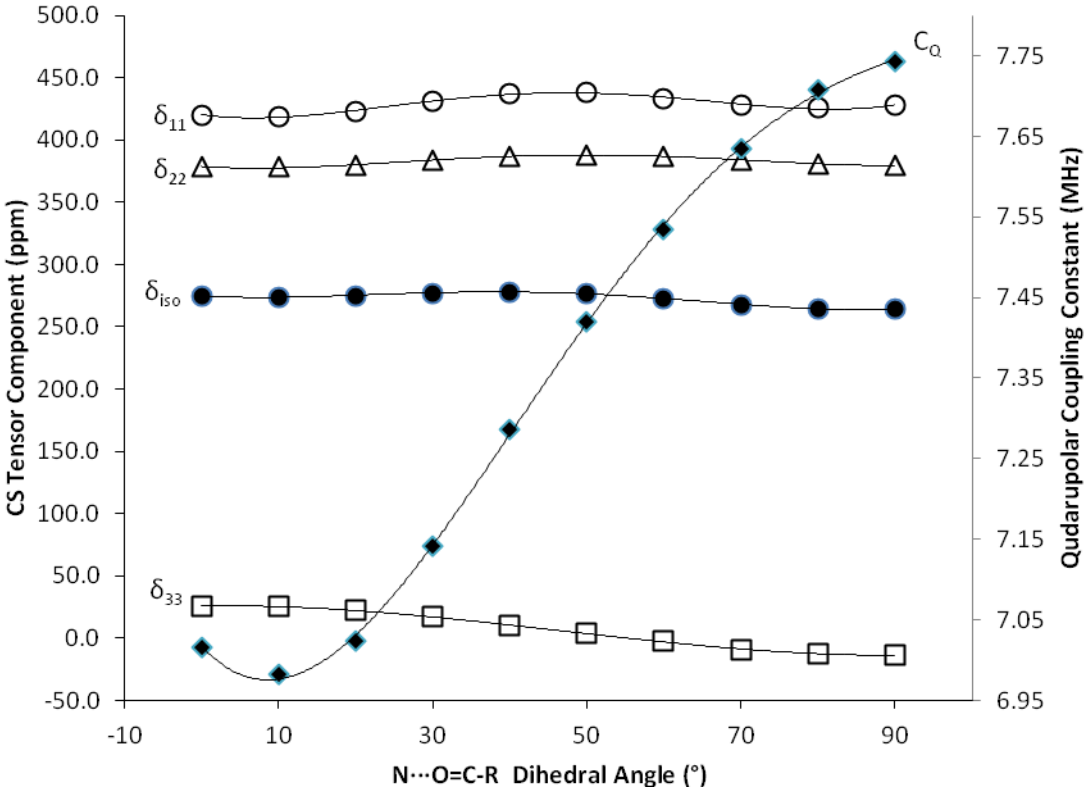

Figure 3.15: Chemical shift tensor components, δ_{iso}, δ_{11}, δ_{22}, δ_{33}, and quadrupolar coupling constant, C_Q, as a function of N···O=C-R dihedral angle, Θ.

Both δ_{11} and δ_{22} exhibit complex relationships with Θ. At Θ = 10°, both tensor components decrease to a local minimum of 418.8 and 378.3 ppm, respectively. They then increase as a function of Θ until Θ = 50°, where they reach a local maximum of 438.3 and 388.3 ppm. δ_{33}, after which they decrease steadily as a function of Θ, from 25.6 ppm at Θ = 0° to -13.9 ppm at Θ = 90°. This leads the isotropic chemical shift to initially increase as a function of Θ, but then decrease again past Θ = 40°, covering a range of approximately 13 ppm. Though the individual tensor components exhibit a smaller range in chemical shifts from changing Θ than from altering the hydrogen bond distances, the resultant impact on isotropic chemical shift from both factors is of similar

magnitude. The most interesting feature in Figure 3.15 is that the ^{17}O quadrupolar coupling constant exhibit a higher sensitivity toward Θ than the chemical shift tensor components. For example, C_Q has a local minimum of 6.98 MHz at Θ = 10°, before steadily increasing as a function of Θ, up to 7.74 MHz at Θ = 90°. This span of 0.7 MHz is similar to that found from altering hydrogen bond distances, where C_Q ranged from 7.02 MHz at 2.5 Å to 7.70 MHz at 3.2 Å (Figure 3.12). By comparison, for δ_{iso} we observe a range of 13.6 ppm from varying Θ, while a change of 17.4 ppm was observed when varying H-bond distance from 2.5 Å to 3.2 Å.

This suggests that while both ^{17}O quadrupolar coupling constant and chemical shift tensor display similar sensitivity to hydrogen bond length, the former is more sensitive to the hydrogen bond direction than the latter. This difference in sensitivity is potentially useful in probing different aspects of the hydrogen bond geometry.

3.4.4 An Acyl-Enzyme Model Based on Crystallographic Data

Having examined the effects of hydrogen bond distance and direction on ^{17}O NMR parameters in isolation, we set out to build a more complex model to mimic the hydrogen bonding environment around the oxyanion hole in real enzymes. To this end, we first surveyed a number of acyl-enzyme complexes of closely related serine proteases available in the Research Collaboratory for Structural Bioinformatics Protein Data Bank (RCSB PDB). (Table 3.5) After careful examination of the current literature crystallographic data, we identified two structural parameters – the C^{β}-O^{γ}-C_1 bond angle (θ) and the C^{α}-C^{β}-O^{γ}-C_1 dihedral angle (φ) (shown in Figure 3.16) – as the major variables with the biggest impact on the placement of the carbonyl oxygen atom in the oxyanion hole. Our survey revealed that the bond angle θ ranges from 114° to 131° and the dihedral angle φ ranges from 83° to 110°. As a result, the O···N hydrogen bond lengths vary between 2.4 Å and 3.5 Å to both Ser195 and Gly193 backbone amide nitrogen atoms.

Table 3.5: Structural data of some acyl-enzyme intermediates of serine proteases. The crystal structure used as an input in the computational study in this thesis is bolded.

Structure	PDB ID	Resolution (Å)	HB distances (Å)		θ (°)	φ (°)
			Gly193	Ser195		
A	2GCT[64]	1.80	3.253	2.452	131	87
B	1GMC[65]	2.20	3.046	2.952	119	100
C	**1K2I[66]**	**1.80**	**3.405**	**2.990**	**120**	**110**
D	1AB9[67]	1.60	3.459 2.887	2.986 2.762	127 117	101 85
E	1HAX[35]	1.60	2.806	2.729	124	83
F	1GVK[68]	0.94	2.723	2.849	117	89
G	2AGE[69]	1.15	2.855	3.016	120	91
H	1XVM[70]	1.10	2.965	2.836	121	94
I	2AH4[69]	1.13	3.142	3.454	118	98
J	1GBT[71]	2.00	3.280	3.409	114	102
K	2AGI[72]	1.14	2.776	3.171	117	109

The enzyme and the bound peptide or small-molecule inhibitor are represented by the structure code as follows:
A: γ-chymotrypsin, PGAY
B: γ-chymotrypsin, PGAY
C: γ-chymotrypsin, 2,4-dihydroxy-*trans*-cinnamic acid
D: γ-chymotrypsin, TPGVY (hetero-dimer with different active site geometries reported)
E: elastase, β-casomorphin-7
F: elastase, acetyl-NPI
G: trypsin, succinyl-AAPR
H: trypsin, GAR
I: trypsin, guanidinobenzoic acid
J: trypsin, guanidinobenzoic acid
K: trypsin, leupeptin

The atomic coordinates from the X-ray crystal structure of *trans*-2,4-dihydroxycinnamoyl-γ-chymotrypsin (PDB ID: 1K2I) were used to construct our acyl-enzyme model. The inhibitor in this case, being a cinnamoyl derivative, is structurally similar to the inhibitors - DAB, oMC, and pMC - used in this study. Further γ-chymotrypsin, being a complex of α-chymotrypsin and its autolysis products, shares the identical primary sequence with α-chymotrypsin.[73] To reduce the computational load, only amino acids 192 to 196 were used in the quantum chemical calculation to emulate the environment surrounding the oxyanion hole. Those residues were chosen to extend one residue beyond Gly193 and Ser195, whose backbone hydrogen atoms are responsible for the hydrogen bonding in the oxyanion hole. The C-terminus of Gly196 is terminated with N-methylamide, with the amide nitrogen and the methyl carbon occupying the same position as the backbone N and C^{α} of Gly197 to mimic neighboring peptide backbones. Likewise, the N-terminus of Met192 is terminated with a N-acetyl group, with the carbon atoms occupying the same positions as the backbone carbonyl carbon and C^{α} of Cys191. The *trans*-2,4-dihydroxycinnamoyl inhibitor was replaced with an O-acetyl group (Figure 3.16), so the calculated ^{17}O NMR parameters for the acetyl group would be indicative of the hydrogen bonding interaction in the oxyanion hole.

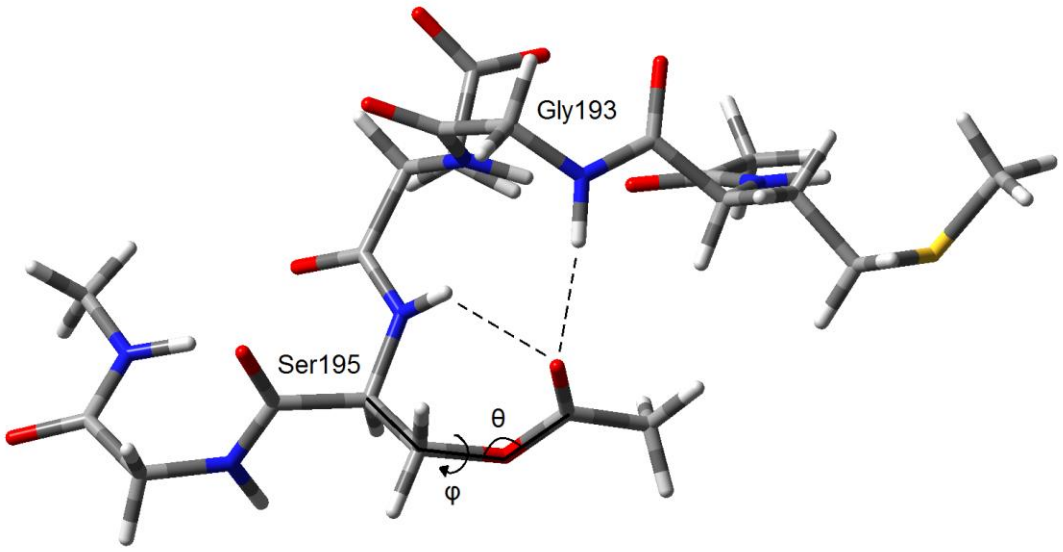

Figure 3.16: Selected amino acid residues in the active site of O-acetyl-γ-chymotrypsin. The two parameters varied in the computational studies – the C^{α}-C^{β}-O^{γ}-C_1 dihedral angle (φ), and C^{β}-O^{γ}-C_1 bond angle (θ) - are noted. The oxyanion hole is formed by the backbone amide protons of serine-195 and glycine-193, shown here forming hydrogen bonds with the carbonyl oxygen.

We explored how ^{17}O NMR parameters changed as a function of the two defined angles. The bond angle θ was varied from 100° to 130°, and the dihedral angle φ was varied from 80° to 120°, both in 5° increments, to a total of 63 θ- φ combinations. Before calculating the NMR parameters, a partial geometry optimization (*opt* function in *Gaussian09*) was performed with the three atoms involved in the hydrogen bonding in the oxyanion hole (the two amide hydrogen atoms from the backbone of amino acid residues Ser195 and Gly193, and the carbonyl oxygen, O_1) allowed to move freely, while the remaining atoms were frozen in place. This permits the oxygen atom and the H-bond hydrogen atoms to explore local energy minima without interference from the rest of the model. The calculated C_Q and δ_{iso} are presented in Figure 3.17 a-b).

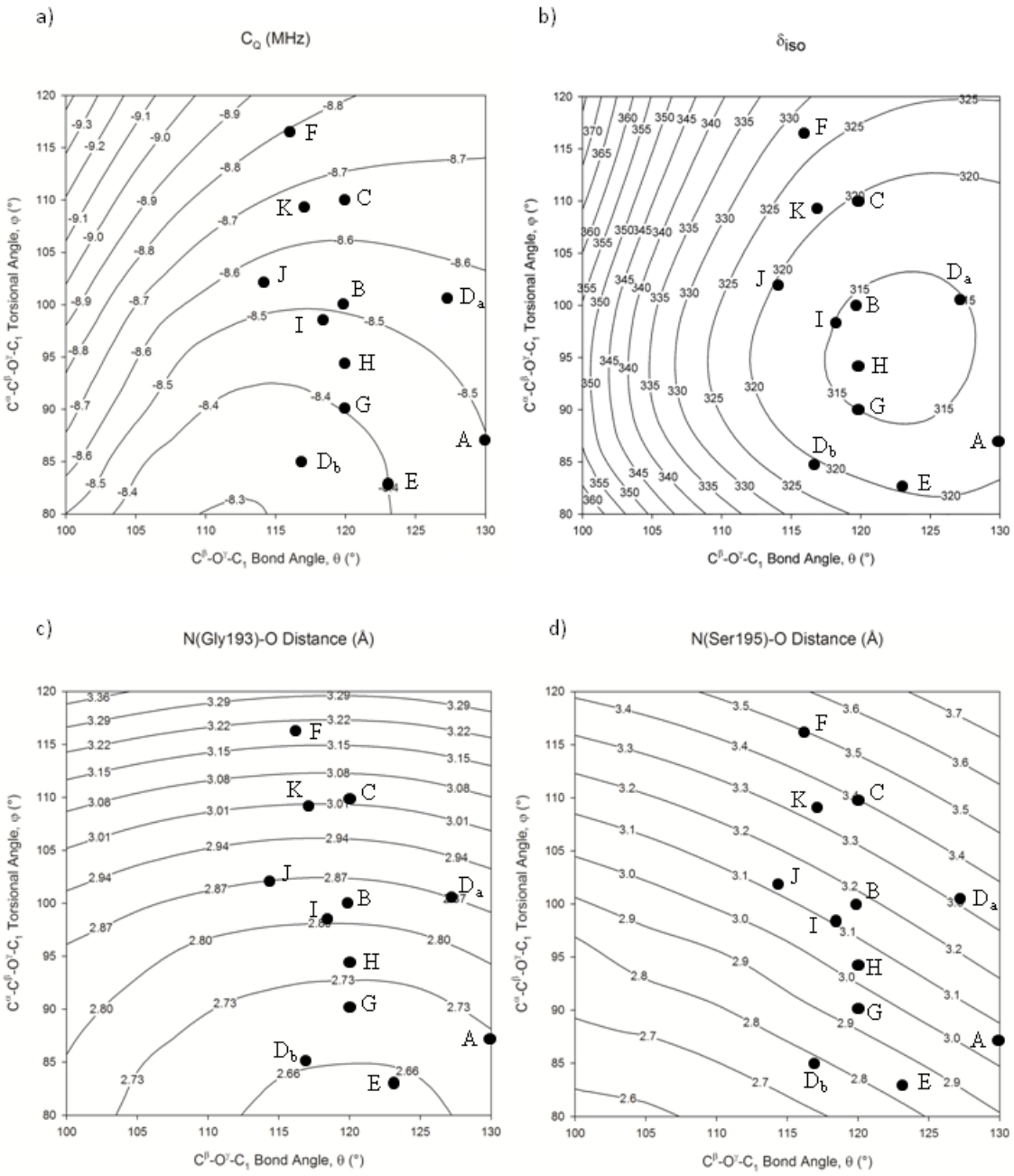

Figure 3.17: Dependences of computed ^{17}O NMR parameters and hydrogen bond distances on the C^{β}-O^{γ}-C_1 bond angle (θ) and the C^{α}-C^{β}-O^{γ}-C_1 dihedral angle (φ). The filled circles indicate the positions from the known acyl-enzyme crystal structures (A-K) listed in Table 3.5.

In the acyl-enzyme model, decreasing the C^{β}-O^{γ}-C_1 bond angle, θ, has the effect of rotating the carbonyl oxygen towards the Ser195 backbone nitrogen and away from the Gly193 backbone nitrogen. Increasing θ brings the oxygen atom closer to N(Gly193), until a local minimum at around 120°, beyond which the distance increases again. Decreasing the C^{α}-C^{β}-O^{γ}-C_1 dihedral angle, φ, turns the carbonyl oxygen atom towards the oxyanion hole, closer to both hydrogen bond donors. The relationship between N(Ser195)-O distance and φ appear independent to its relationship with θ, while a more complex relationship exists for N(Gly193)-O distance. The relationship between these two angles and hydrogen bond distances are summarized in Figure 3.17 c) and d).

On initial examination, the ^{17}O NMR parameters display a dependency on the two angles examined. Since φ effectively determines the distance between the carbonyl oxygen and both hydrogen bond donors, it is no surprise that C_Q decreases as φ decreases, consistent with established trends between C_Q and proximity to the hydrogen bond donors. The effect of θ on C_Q, on the other hand, is more complex. There is a local minimum at θ = 112° and φ = 80°, but at the other extreme of φ = 120° the minimum lies at the extreme of θ = 130°. The similarities between Figure 3.17 a) and c) suggests that distance to N(Gly193) may play a larger role in influencing C_Q than N(Ser195).

The acyl-enzymes with known crystal structures labeled A-K are also displayed on Figure 3.17. We observe that they are clustered around θ = 120°, with a more scattered distribution of φ from 80° – 115°. Interestingly, the center of the cluster roughly coincides with the minimum for δ_{iso}. As δ_{iso} is sensitive to the hydrogen bond distance (and to a lesser degree, orientation; see Section 3.4.3), the minimum represents the angles with the strongest hydrogen bond interactions. One would expect the angles for the

family of serine proteases to fall close to that area in order to maximize catalytic efficiency.

The sensitivity of C_Q and δ_{iso} to both hydrogen bond distance and angle, coupled with the complex relationships between the two angles θ and φ, and the geometry of the hydrogen bonds to Gly193 and Ser195, made quantitative interpretation of the ^{17}O NMR data difficult. Nonetheless, the results presented here serve as a promising start for further computational studies.

Chapter 4

Conclusion and Future Directions

This thesis reports the first use of solid-state ^{17}O NMR spectroscopy to study acyl-enzyme intermediates. In particular, three ^{17}O-enriched acyl-enzyme intermediates, *p*-N,N-dimethylaminobenzoyl-, *trans-o*-methoxycinnamoyl-, and *trans-p*-methoxycinnamoyl-chymotrypsin, were successfully synthesized. In the mass spectra of these acyl-enzymes, we observed major peaks at 25597.2 ± 1.5, 25608.9 ± 0.3, 25609.7 ± 0.6, and 25579.7 ± 0.3 Da, which confirm the formation of acyl-enzymes with the level of acylation in the range of 79% to 95%. The kinetics of deacylation of the three acyl-enzyme intermediates were determined via an enzyme activity assay and UV-vis spectroscopy. The measured rate constants are in good agreement with reported literature values. These deacylation rates suggest that the carbonyl oxygen atom in the oxyanion hole must experience very different hydrogen-bonding environments in the three acyl-enzymes.

By performing solid-state ^{17}O NMR experiments, we have determined the ^{17}O NMR parameters for the three acyl-enzymes. C_Q and η_Q were found to be in the range of 10.0 ± 1 to 7.0 ± 0.5 MHz and 0.6 ± 0.2 to 0.8 ± 0.2, respectively. The principal components of the CS tensor were determined: δ_{11} ranged from 614 ± 10 to 458 ± 10 ppm, δ_{22} ranged from 369 ± 10 to 318 ± 10 ppm, and δ_{33} ranged from -34 ± 10 to 88 ± 10 ppm. δ_{iso} was found to be in the range of 316 ± 2 to 288 ± 2 ppm. The trends exhibited by the NMR parameters reflect the variation in hydrogen-bond strength of the respective acyl-enzymes, as previously demonstrated in Raman studies.

To aid the interpretation of the experimental ^{17}O NMR data, we performed quantum mechanical calculations of the ^{17}O NMR parameters for both simple molecular cluster models and an acyl-enzyme model constructed from the reported crystal structures. In general we demonstrated that both hydrogen bond length and direction have significant impacts on the chemical shift tensor and quadrupolar coupling constant. We conclude that the variations in ^{17}O NMR parameter observed experimentally for the three acyl-enzyme intermediates are due to the different hydrogen bonding environments in the oxyanion hole. The present study demonstrates the feasibility and utility of solid-state ^{17}O NMR in studying a model enzyme. We believe that not only can this work be extended to other serine proteases, but solid-state ^{17}O NMR can provide unique insight into enzyme kinetics and mechanisms in general.

As discussed in Section 3.4.4, further refinement of the acyl-enzyme model based on crystallographic data is required for a meaningful correlation between the geometry of the oxyanion hole and NMR parameters. A logical next step is to obtain crystal structures for the specific acyl-chymotrypsin used for direct comparison with experimentally obtained NMR data. This may help elucidate the geometry information the observed NMR data contains.

Beyond using "poor" substrates with long deaclylation half-lives, as performed in this thesis, mechanistic studies of serine proteases has involved the use of transition state analog inhibitors. These suicide inhibitors react with the active site to form a non-scissile hemiacetal group. ^{17}O NMR on these complexes should be more sensitive to the chemical environment around the catalytic site than other techniques, such as ^{13}C NMR.

Previous work by Wu *et al*[74] has demonstrated a quadrupole central transition (QCT) method that can obtain ^{17}O NMR spectra in the solution state for a protein with a given molecular rotational correlation time. By a careful choice of substrates, many aqueous acyl-enzymes can have deacylation half-lives on the order of hours to tens of hours, long enough to allow for solution-state ^{17}O NMR spectroscopy and greatly expanding the possible applications of this technique.

A further application of ^{17}O NMR in studying acyl-enzymes is in enzymes of pharmaceutical interest. As a large number of drugs target enzymes, with many doing so via irreversible inhibition through reactive chemistry at the active site, the ability to directly probe the atoms involved in the mechanism provides an additional technique to aid in rational drug design. The same methodology can be applied to other drug targets, such as receptors, where non-covalent interactions can also be investigated via ^{17}O NMR.

References

1. Wu, G., Solid-state 17O NMR studies of organic and biological molecules. *Prog. Nucl. Magn. Reson. Spectrosc.* **2008,** *52* (2), 118-169; Dahn, H.; Carrupt, P.-A., The Origin of the Difference Between the ^{13}C and ^{17}O Shift Behaviour of Carbonyl Compounds RCOX:Ab initio Calculation of the Shielding Tensors. *Magn. Reson. Chem.* **1997,** *35* (9), 577-588.

2. Alder, F.; Yu, F., On the Spin and Magnetic Moment of O^{17}. *Phys. Rev.* **1951,** *81* (6), 1067-1068.

3. Goc, R.; Ponnusamy, E.; Tritt-Goc, J.; Fiat, D., ^{17}O n.m.r. studies of amino acids in the solid state, in single- and polycrystalline forms. *Int. J. Pept. Protein Res.* **1988,** *31* (2), 130-6.

4. Wu, G.; Dong, S., Two-Dimensional ^{17}O Multiple Quantum Magic-Angle Spinning NMR of Organic Solids. *J. Am. Chem. Soc.* **2001,** *123* (37), 9119-9125.

5. Lemaitre, V.; Pike, K. J.; Watts, A.; Anupold, T.; Samoson, A.; Smith, M. E.; Dupree, R., New insights into the bonding arrangements of l- and d-glutamates from solid state ^{17}O NMR. *Chem. Phys. Lett.* **2003,** *371* (1-2), 91-97.

6. Oldfield, E.; Lee, H. C.; Coretsopoulos, C.; Adebodun, F.; Park, K. D.; Yang, S.; Chung, J.; Phillips, B., Solid-state oxygen-17 nuclear magnetic resonance spectroscopic studies of [$^{17}O_2$] picket fence porphyrin, myoglobin, and hemoglobin. *J. Am. Chem. Soc.* **1991,** *113* (23), 8680-8685.

7. Collman, J. P.; Gagne, R. R.; Reed, C. A.; Robinson, W. T.; Rodley, G. A., Structure of an iron(II) dioxygen complex; a model for oxygen carrying hemeproteins. *Proc. Natl. Acad. Sci. USA* **1974,** *71* (4), 1326-9.

8. Kaupp, M.; Rovira, C.; Parrinello, M., Density Functional Study of ^{17}O NMR Chemical Shift and Nuclear Quadrupole Coupling Tensors in Oxyheme Model Complexes. *J. Phys. Chem. B* **2000,** *104* (21), 5200-5208.

9. Wu, G.; Dong, S.; Ida, R.; Reen, N., A Solid-State ^{17}O Nuclear Magnetic Resonance Study of Nucleic Acid Bases. *J. Am. Chem. Soc.* **2002,** *124* (8), 1768-1777.

10. Kuroki, S.; Takahashi, A.; Ando, I.; Shoji, A.; Ozaki, T., Hydrogen-bonding structural study of solid peptides and polypeptides containing a glycine residue by ^{17}O NMR spectroscopy. *J. Mol. Struct.* **1994,** *323*, 197-208.

11. Kuroki, S.; Ando, S.; Ando, I., An MO study of nuclear quadrupolar coupling constant and nuclear shielding of the carbonyl oxygen in solid peptides with hydrogen bonds. *Chem. Phys.* **1995,** *195* (1-3), 107-116.

12. Wu, G.; Yamada, K.; Dong, S.; Grondey, H., Intermolecular hydrogen-bonding effects on the amide oxygen electric-field-gradient and chemical shielding tensors of benzamide. *J. Am. Chem. Soc.* **2000,** *122* (17), 4215-4216; Yamada, K.; Dong, S.; Wu, G., Solid-State ^{17}O NMR Investigation of the Carbonyl Oxygen Electric-Field-Gradient Tensor and Chemical Shielding Tensor in Amides. *J. Am. Chem. Soc.* **2000,** *122* (47), 11602-11609.

13. de Dios, A. C.; Oldfield, E., Chemical Shifts of Carbonyl Carbons in Peptides and Proteins. *J. Am. Chem. Soc.* **1994,** *116* (25), 11485-11488.

14. Wu, G.; Dong, S.; Ida, R., Solid-state ^{17}O NMR of thymine: a potential new probe to nucleic acid base pairing. *Chem. Commun.* **2001,** (10), 891-892.

15. Dong, S.; Ida, R.; Wu, G., A Combined Experimental and Theoretical ^{17}O NMR Study of Crystalline Urea: An Example of Large Hydrogen-bonding Effects. *J. Phys. Chem. A* **2000,** *104* (47), 11194-11202.

16. Butler, L. G.; Brown, T. L., Nuclear quadrupole coupling constants and hydrogen bonding. Molecular orbital study of oxygen-17 and deuterium field gradients in formaldehyde-water hydrogen bonding. *J. Am. Chem. Soc.* **1981,** *103* (22), 6541-6549.

17. Butler, L. G.; Cheng, C. P.; Brown, T. L., Oxygen-17 nuclear quadrupole double resonance. 6. Effects of hydrogen bonding. *J. Phys. Chem.* **1981,** *85* (19), 2738-2740.

18. Gready, J. E., Theoretical study of the variability of the electric field gradient tensor of oxygen nuclei in organic molecules. *J. Phys. Chem.* **1984,** *88* (16), 3497-3503.

19. Pake, G. E., Nuclear Resonance Absorption in Hydrated Crystals: Fine Structure of the Proton Line. *J. Chem. Phys* **1948,** *16* (4), 327.

20. Andrew, E.; Bradbury, A.; Eades, R., Removal of dipolar broadening of nuclear magnetic resonance spectra of solids by specimen rotation. *Nature* **1959**.

21. Lowe, I. J., Free Induction Decays of Rotating Solids. *Phys. Rev. Lett.* **1959,** *2* (7), 285-287.

22. Schramm, S.; Kirkpatrick, R. J.; Oldfield, E., Observation of high-resolution oxygen-17 NMR spectra of inorganic solids. *J. Am. Chem. Soc.* **1983,** *105* (8), 2483-2485; Schramm, S.; Oldfield, E., High-resolution oxygen-17 NMR of solids. *J. Am. Chem. Soc.* **1984,** *106* (9), 2502-2506.

23. Haldane, J. B. S., *Enzymes*. Longmans, Green: London, 1930.

24. Cornish-Bowden, A., History of Enzyme Chemistry. **2011**.

25. Kraut, J., How Do Enzymes Work? *Science* **1988,** *242* (4878), 533-540.

26. Fischer, E., Influence of configuration on the action of enzymes. *Ber. Dtsch. Chem. Ges.* **1894,** *27*, 2985-2993.

27. Lichtenthaler, F. W., 100 Years“Schlüssel-Schloss-Prinzip”: What Made Emil Fischer Use this Analogy? *Angew. Chem. Int. Ed.* **1995,** *33* (2324), 2364-2374.

28. Eyring, H., The Activated Complex in Chemical Reactions. *J. Chem. Phys* **1935,** *3* (2), 107-115.

29. Pauling, L., Chemical achievement and hope for the future. *Am. Sci.* **1948,** *36* (1), 51-8.

30. Bernhard, S. A.; Orgel, L. E., Mechanism of enzyme inhibition by phosphate esters. *Science* **1959,** *130* (3376), 625-6.

31. Wolfenden, R., Transition State Analogues for Enzyme Catalysis. *Nature* **1969,** *223* (5207), 704-705; Wolfenden, R., Analog approaches to the structure of the transition state in enzyme reactions. *Acc. Chem. Res.* **1972,** *5* (1), 10-18; Lienhard, G. E., Chapter 23. Transition State Analogs as Enzyme Inhibitors. **1972,** *7*, 249-258; Lienhard, G. E., Enzymatic catalysis and transition-state theory. *Science* **1973,** *180* (4082), 149-54.

32. Blake, C. C. F.; Johnson, L. N.; Mair, G. A.; North, A. C. T.; Phillips, D. C.; Sarma, V. R., Crystallographic Studies of the Activity of Hen Egg-White Lysozyme. *Proc. R. Soc. B* **1967,** *167* (1009), 378-388; Blake, C. C. F.; Koenig, D. F.; Mair, G. A.; North, A. C. T.; Phillips, D. C.; Sarma, V. R., Structure of Hen Egg-White Lysozyme: A Three-dimensional Fourier Synthesis at 2 Å Resolution. *Nature* **1965,** *206* (4986), 757-761; Phillips, D. C., The Hen Egg-White Lysozyme Molecule. *Proc. Natl. Acad. Sci. USA* **1967,** *57* (3), 483-495.

33. Johnson, L. N.; Phillips, D. C., Structure of Some Crystalline Lysozyme-Inhibitor Complexes Determined by X-Ray Analysis At 6 Å Resolution. *Nature* **1965,** *206* (4986), 761-763.

34. Kraut, J., Serine proteases: structure and mechanism of catalysis. *Ann. Rev. Biochem.* **1977,** *46*, 331-58; Wilmouth, R. C.; Westwood, N. J.; Anderson, K.; Brownlee, W.; Claridge, T. D. W.; Clifton, I. J.; Pritchard, G. J.; Aplin, R. T.; Schofield, C. J., Inhibition of Elastase by N-Sulfonylaryl β-Lactams: Anatomy of a Stable Acyl−Enzyme Complex†,‡. *Biochemistry* **1998,** *37* (50), 17506-17513.

35. Wilmouth, R. C.; Edman, K.; Neutze, R.; Wright, P. A.; Clifton, I. J.; Schneider, T. R.; Schofield, C. J.; Hajdu, J., X-ray snapshots of serine protease catalysis reveal a tetrahedral intermediate. *Nat. Struct. Biol.* **2001,** *8* (8), 689-94.

36. Hedstrom, L., Serine protease mechanism and specificity. *Chem. Rev.* **2002,** *102* (12), 4501-4524.

37. Blow, D. M.; Birktoft, J. J.; Hartley, B. S., Role of a buried acid group in the mechanism of action of chymotrypsin. *Nature* **1969,** *221* (5178), 337-40.

38. Robillard, G.; Shulman, R. G., High resolution nuclear magnetic resonance study of the histidine--aspartate hydrogen bond in chymotrypsin and chymotrypsinogen. *J Mol Biol* **1972,** *71* (2), 507-11.

39. Bachovchin, W. W., Confirmation of the Assignment of the Low-Field Proton Resonance of Serine Proteases by Using Specifically Nitrogen-15 Labeled Enzyme. *Proc. Natl. Acad. Sci. USA* **1985,** *82* (23), 7948-7951.

40. Bachovchin, W. W., Nitrogen-15 NMR spectroscopy of hydrogen-bonding interactions in the active site of serine proteases: evidence for a moving histidine mechanism. *Biochemistry* **1986,** *25* (23), 7751-7759.

41. Tsilikounas, E.; Kettner, C. A.; Bachovchin, W. W., Boron-11 NMR spectroscopy of peptide boronic acid inhibitor complexes of .alpha.-lytic protease. Direct evidence for tetrahedral boron in both boron-histidine and boron-serine adduct complexes. *Biochemistry* **1993,** *32* (47), 12651-12655.

42. Henderson, R., Structure of crystalline α-chymotrypsin: IV. The structure of indoleacryloyl-α-chymotrypsin and its relevance to the hydrolytic mechanism of the enzyme. *J. Mol. Biol.* **1970,** *54* (2), 341-354.

43. Corey, D. R.; Craik, C. S., An investigation into the minimum requirements for peptide hydrolysis by mutation of the catalytic triad of trypsin. *J. Am. Chem. Soc.* **1992,** *114* (5), 1784-1790; Carter, P.; Wells, J. A., Dissecting the catalytic triad of a serine protease. *Nature* **1988,** *332* (6164), 564-8.

44. Tonge, P. J.; Carey, P. R., Direct observation of the titration of substrate carbonyl groups in the active site of .alpha.-chymotrypsin by resonance Raman spectroscopy. *Biochemistry* **1989,** *28* (16), 6701-6709; Tonge, P. J.; Carey, P. R., Length of the acyl carbonyl bond in acyl-serine

proteases correlates with reactivity. *Biochemistry* **1990,** *29* (48), 10723-10727; Tonge, P. J.; Carey, P. R., Forces, bond lengths, and reactivity: fundamental insight into the mechanism of enzyme catalysis. *Biochemistry* **1992,** *31* (38), 9122-9125; Tonge, P. J.; Pusztai, M.; White, A. J.; Wharton, C. W.; Carey, P. R., Resonance Raman and Fourier transform infrared spectroscopic studies of the acyl carbonyl group in [3-(5-methyl-2-thienyl)acryloyl]chymotrypsin: evidence for artifacts in the spectra obtained by both techniques. *Biochemistry* **1991,** *30* (19), 4790-4795.

45. Hartley, B.; Kilby, B., The reaction of p-nitrophenyl esters with chymotrypsin and insulin. *J. Biochem.* **1954,** *56* (2), 288.

46. Wirnt, R., Chymotrypsin. In *Methods of Enzymatic Analysis*, 1974; pp 1009-1012.

47. Massiot, D.; Fayon, F.; Capron, M.; King, I.; Le Calvé, S.; Alonso, B.; Durand, J.-O.; Bujoli, B.; Gan, Z.; Hoatson, G., Modelling one- and two-dimensional solid-state NMR spectra. *Magn. Reson. Chem.* **2002,** *40* (1), 70-76.

48. Wu, G.; Hook, A.; Dong, S.; Yamada, K., A Solid-State NMR and Theoretical Study of the ^{17}O Electric Field Gradient and Chemical Shielding Tensors of the Oxonium Ion inp-Toluenesulfonic Acid Monohydrate. *J. Phys. Chem. A* **2000,** *104* (17), 4102-4107.

49. Ashton, D. S.; Beddell, C. R.; Cooper, D. J.; Green, B. N.; Oliver, R. W. A.; Welham, K. J., Some electrospray mass spectrometric evidence for the existence of covalentO-acyl enzyme intermediates. *FEBS Lett.* **1991,** *292* (1–2), 201-204.

50. Ashton, D. S.; Beddell, C. R.; Cooper, D. J.; Green, B. N.; Oliver, R. W. A.; Welham, K. J., On the Purity of 3X-Recrystallised Bovine α-Chymotrypsin. *Biochem. Biophys. Res. Commun.* **1993,** *192* (1), 75-81.

51. Bender, M. L.; Killheffer, J. V.; Cohen, S., Chymotrypsin. *Crit. Rev. Biochem. Mol. Biol.* **1973,** *1* (2), 149-199.

52. Krigbaum, W. R.; Godwin, R. W., Molecular conformation of chymotrypsinogen and chymotrypsin by low-angle x-ray diffraction. *Biochemistry* **1968,** *7* (9), 3126-31.

53. Whiting, A. K.; Peticolas, W. L., Details of the acyl-enzyme intermediate and the oxyanion hole in serine protease catalysis. *Biochemistry* **1994,** *33* (2), 552-561.

54. Sasaki, T.; Kise, H., Effects of Metal Salts on the Structure and Activity of .ALPHA.-Chymotrypsin in Ethanol/Water. *Bull. Chem. Soc. Jpn.* **1999,** *72* (6), 1321-1325.

55. Kumar, S.; Hein, G. E., Mechanism of autolysis of α-chymotrypsin. *Biochemistry* **1970,** *9* (2), 291-297.

56. Bender, M. L.; Schonbaum, G. R.; Zerner, B., Spectrophotometric Investigations of the Mechanism of α-Chymotrypsin-catalyzed Hydrolyses. Detection of the Acyl-enzyme Intermediate1-3. *J. Am. Chem. Soc.* **1962,** *84* (13), 2540-2550.

57. Schonbaum, G. R.; Zerner, B.; Bender, M. L., The Spectrophotometric Determination of the Operational Normality of an α-Chymotrypsin Solution. *J. Biol. Chem.* **1961,** *236* (11), 2930-2935.

58. Bernhard, S. A.; Hershberger, E.; Keizer, J., The Influence of pH on the Rate of Hydrolysis of Acylchymotrypsins*. *Biochemistry* **1966,** *5* (12), 4120-4126.

59. Gready, J. E., The relationship between nuclear quadrupole coupling constants and the asymmetry parameter. The interplay of theory and experiment. *J. Am. Chem. Soc.* **1981,** *103* (13), 3682-3691.

60. Taylor, R.; Kennard, O.; Versichel, W., Geometry of the imino-carbonyl (N-H...O:C) hydrogen bond. 1. Lone-pair directionality. *J. Am. Chem. Soc.* **1983,** *105* (18), 5761-5766.

61. Asakawa, N.; Kuroki, S.; Kurosu, H.; Ando, I.; Shoji, A.; Ozaki, T., Hydrogen-bonding effect on carbon-13 NMR chemical shifts of L-alanine residue carbonyl carbons of peptides in the solid state. *J. Am. Chem. Soc.* **1992,** *114* (9), 3261-3265.

62. Ando, S.; Ando, I.; Shoji, A.; Ozaki, T., Intermolecular hydrogen-bonding effect on carbon-13 NMR chemical shifts of glycine residue carbonyl carbons of peptides in the solid state. *J. Am. Chem. Soc.* **1988,** *110* (11), 3380-3386.

63. Simón, L.; Goodman, J. M., Enzyme Catalysis by Hydrogen Bonds: The Balance between Transition State Binding and Substrate Binding in Oxyanion Holes. *J. Org. Chem.* **2009,** *75* (6), 1831-1840.

64. Dixon, M. M.; Brennan, R. G.; Matthews, B. W., Structure of Gamma-Chymotrypsin in the Range Ph 2.0 to Ph 10.5 Suggests That Gamma-Chymotrypsin Is a Covalent Acyl Enzyme Adduct at Low Ph. *Int. J. Biol. Macromol.* **1991,** *13* (2), 89-96.

65. Yennawar, N. H.; Yennawar, H. P.; Farber, G. K., X-ray crystal structure of gamma-chymotrypsin in hexane. *Biochemistry* **1994,** *33* (23), 7326-36.

66. Ghani, U.; Ng, K. K.; Atta ur, R.; Choudhary, M. I.; Ullah, N.; James, M. N., Crystal structure of gamma-chymotrypsin in complex with 7-hydroxycoumarin. *J Mol Biol* **2001,** *314* (3), 519-25.

67. Kashima, A.; Inoue, Y.; Sugio, S.; Maeda, I.; Nose, T.; Shimohigashi, Y., X-ray crystal structure of a dipeptide-chymotrypsin complex in an inhibitory interaction. *Eur. J. Biochem.* **1998,** *255* (1), 12-23.

68. Katona, G.; Wilmouth, R. C.; Wright, P. A.; Berglund, G. I.; Hajdu, J.; Neutze, R.; Schofield, C. J., X-ray structure of a serine protease acyl-enzyme complex at 0.95-A resolution. *J. Biol. Chem.* **2002,** *277* (24), 21962-70.

69. Radisky, E. S.; Lee, J. M.; Lu, C.-J. K.; Koshland, D. E., Insights into the serine protease mechanism from atomic resolution structures of trypsin reaction intermediates. *Proc. Natl. Acad. Sci. USA* **2006,** *103* (18), 6835-6840.

70. Schmidt, A.; Lamzin, V. S., Extraction of functional motion in trypsin crystal structures. *Acta Crystallogr D* **2005,** *61* (Pt 8), 1132-9.

71. Mangel, W. F.; Singer, P. T.; Cyr, D. M.; Umland, T. C.; Toledo, D. L.; Stroud, R. M.; Pflugrath, J. W.; Sweet, R. M., Structure of an acyl-enzyme intermediate during catalysis: (guanidinobenzoyl)trypsin. *Biochemistry* **1990,** *29* (36), 8351-7.

72. Mosbacher, T. G.; Mueller, M.; Schulz, G. E., Structure and mechanism of the ThDP-dependent benzaldehyde lyase from Pseudomonas fluorescens. *FEBS J.* **2005,** *272* (23), 6067-76.

73. Harel, M.; Su, C. T.; Frolow, F.; Silman, I.; Sussman, J. L., .gamma.-Chymotrypsin is a complex of .alpha.-chymotrypsin with its own autolysis products. *Biochemistry* **1991,** *30* (21), 5217-5225.

74. Zhu, J.; Kwan, I. C. M.; Wu, G., Quadrupole-Central-Transition ^{17}O NMR Spectroscopy of Protein−Ligand Complexes in Solution. *J. Am. Chem. Soc.* **2009,** *131* (40), 14206-14207.

Appendix A

Supplemental Data

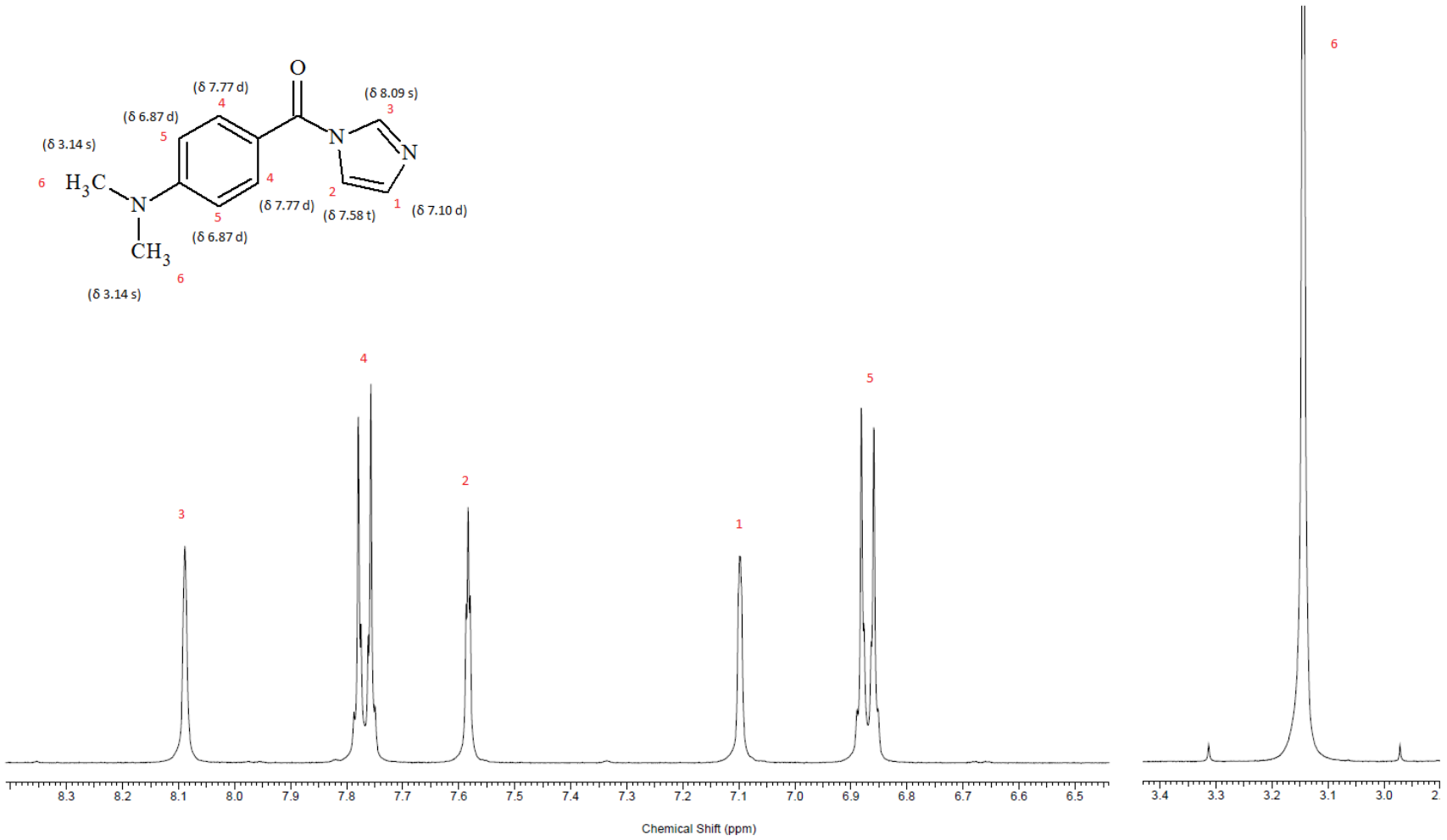

Figure A- 1: ^{1}H NMR spectrum of *p*-N,N-dimethylaminobenoylimidazole (DAB-Im) in $CD_3(CO)CD_3$ at 9.4 T, 298 K.

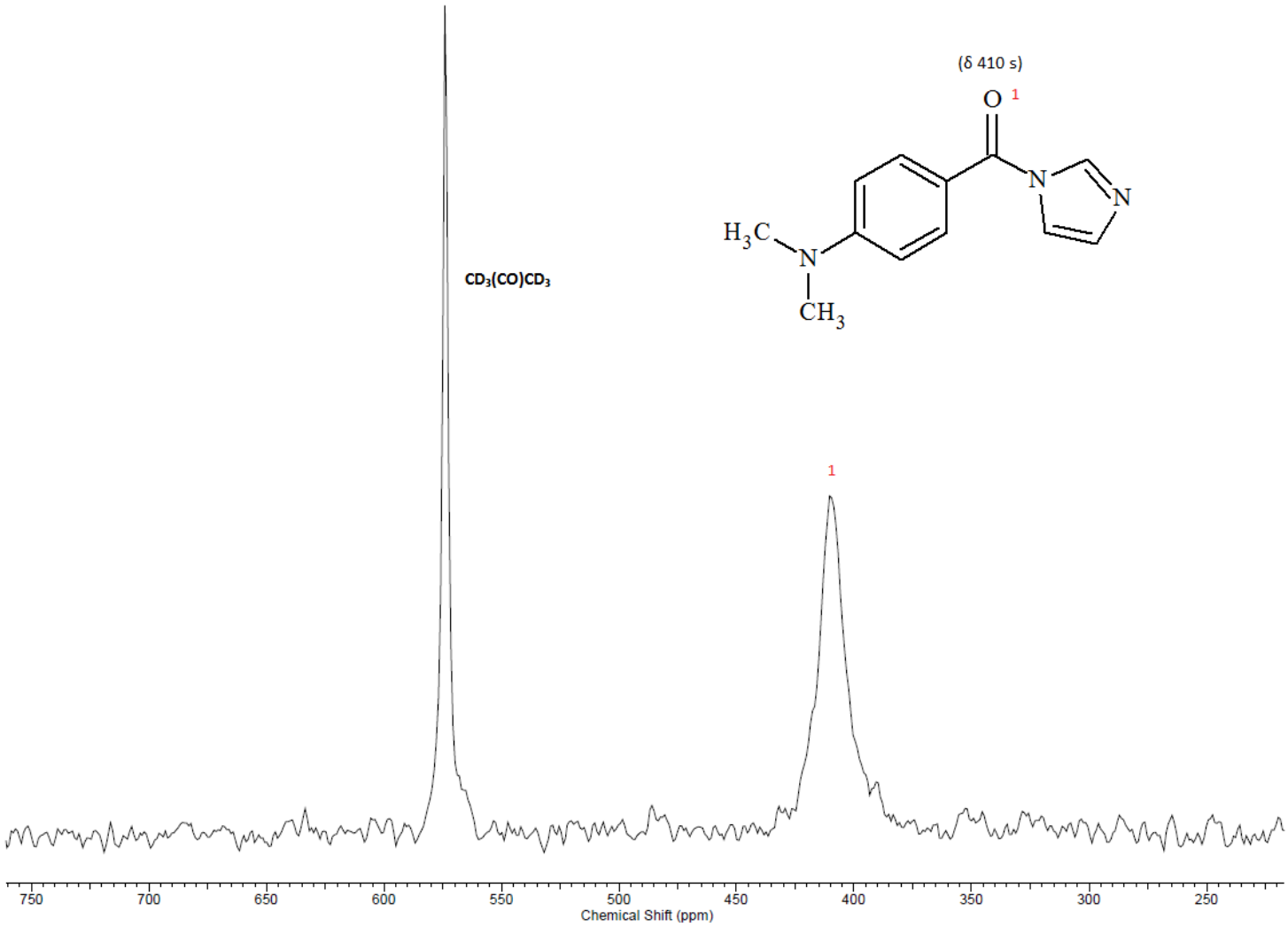

Figure A- 2: ^{17}O NMR spectrum of *p*-N,N-dimethylamino-[^{17}O]benoylimidazole in $CD_3(CO)CD_3$ at 9.4 T, 298 K.

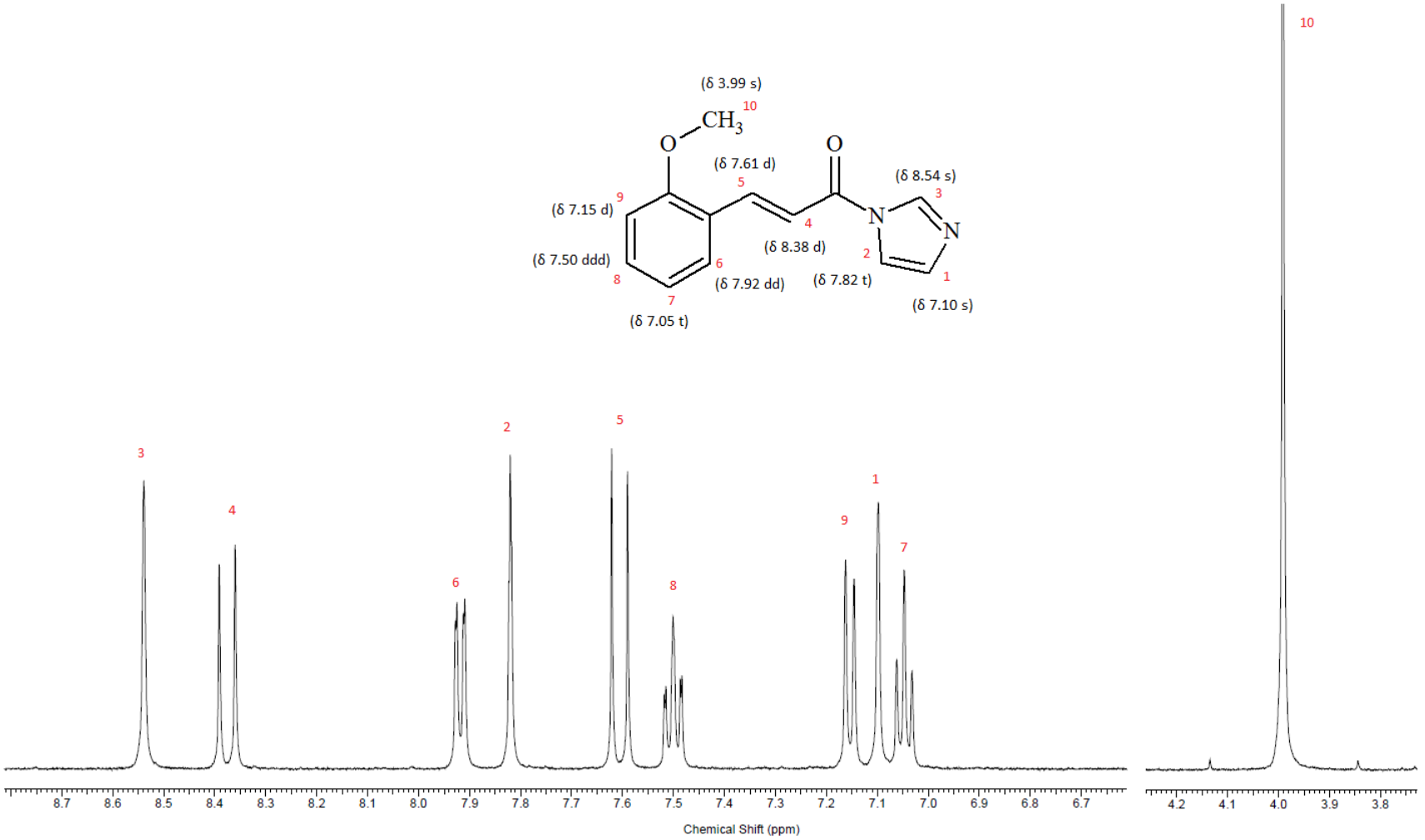

Figure A- 3: ^{1}H NMR spectrum of *trans-o*-methoxycinnamoylimidazole in acetone-d6.

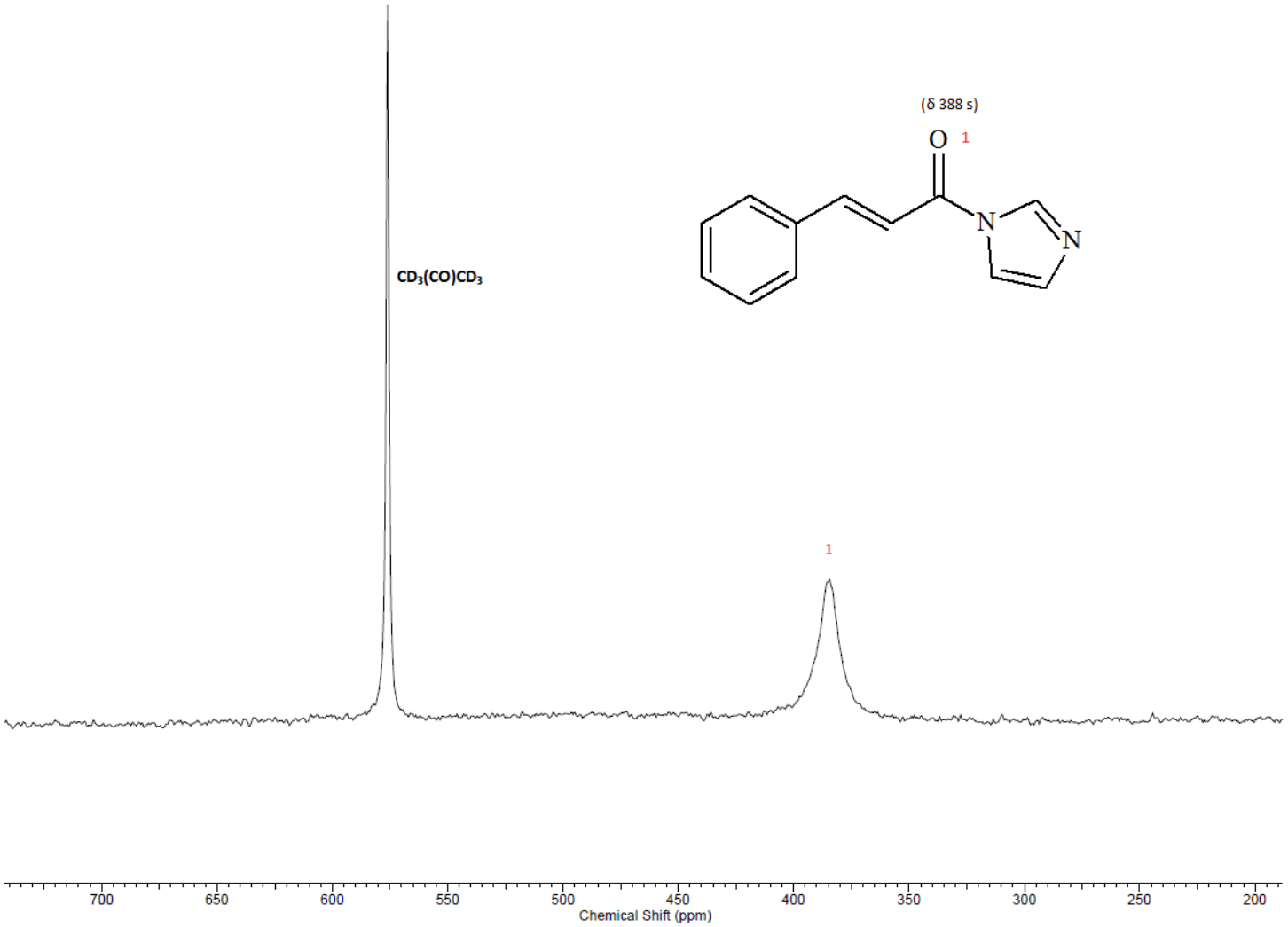

Figure A- 4: ^{17}O-NMR Spectrum of *trans*-*o*-methoxycinnamoylimidazole

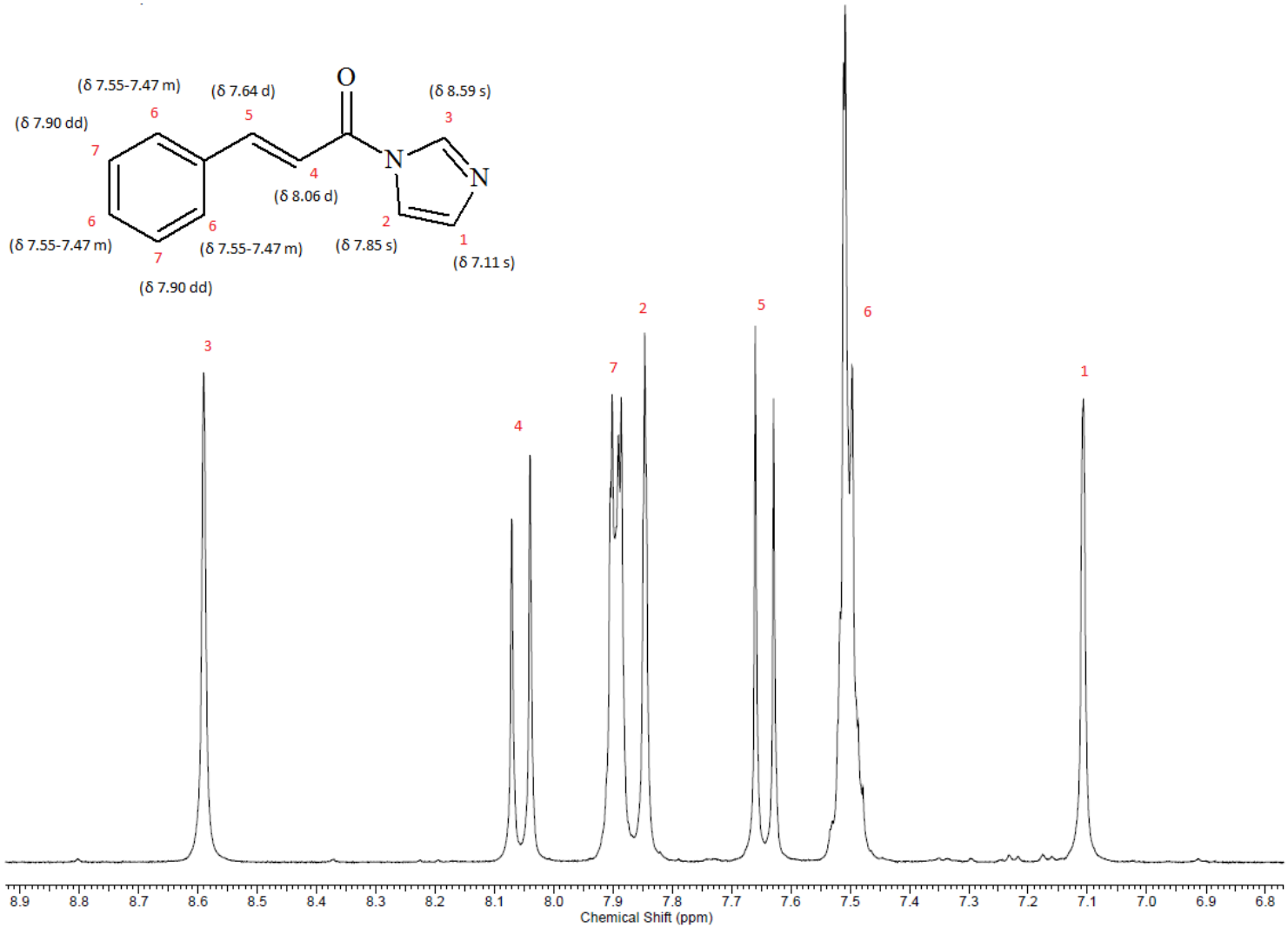

Figure A- 5: ^{1}H-NMR Spectrum of *trans*-cinnamoylimidazole

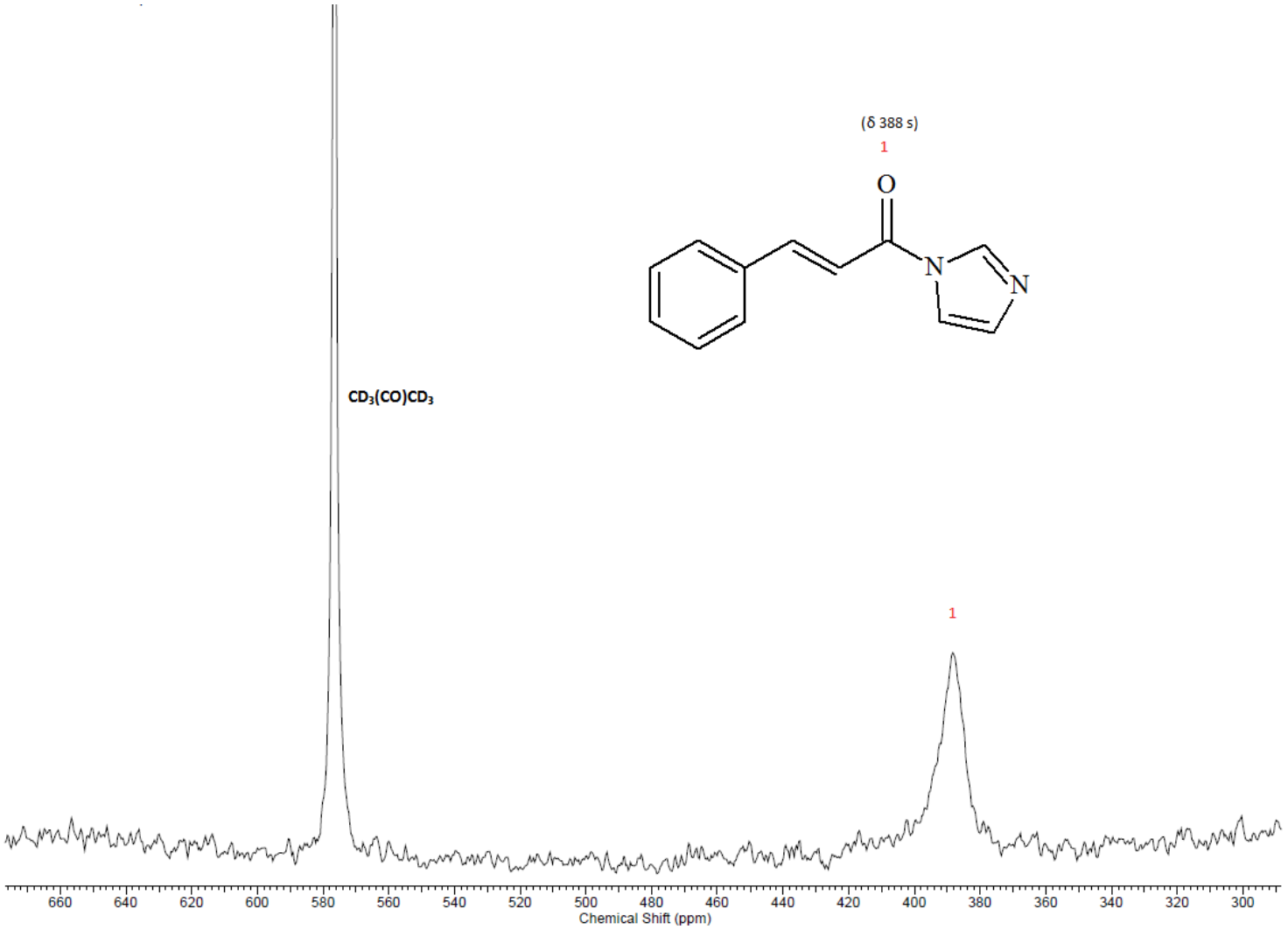

Figure A- 6: ^{17}O-NMR Spectrum of *trans*-cinnamoylimidazole

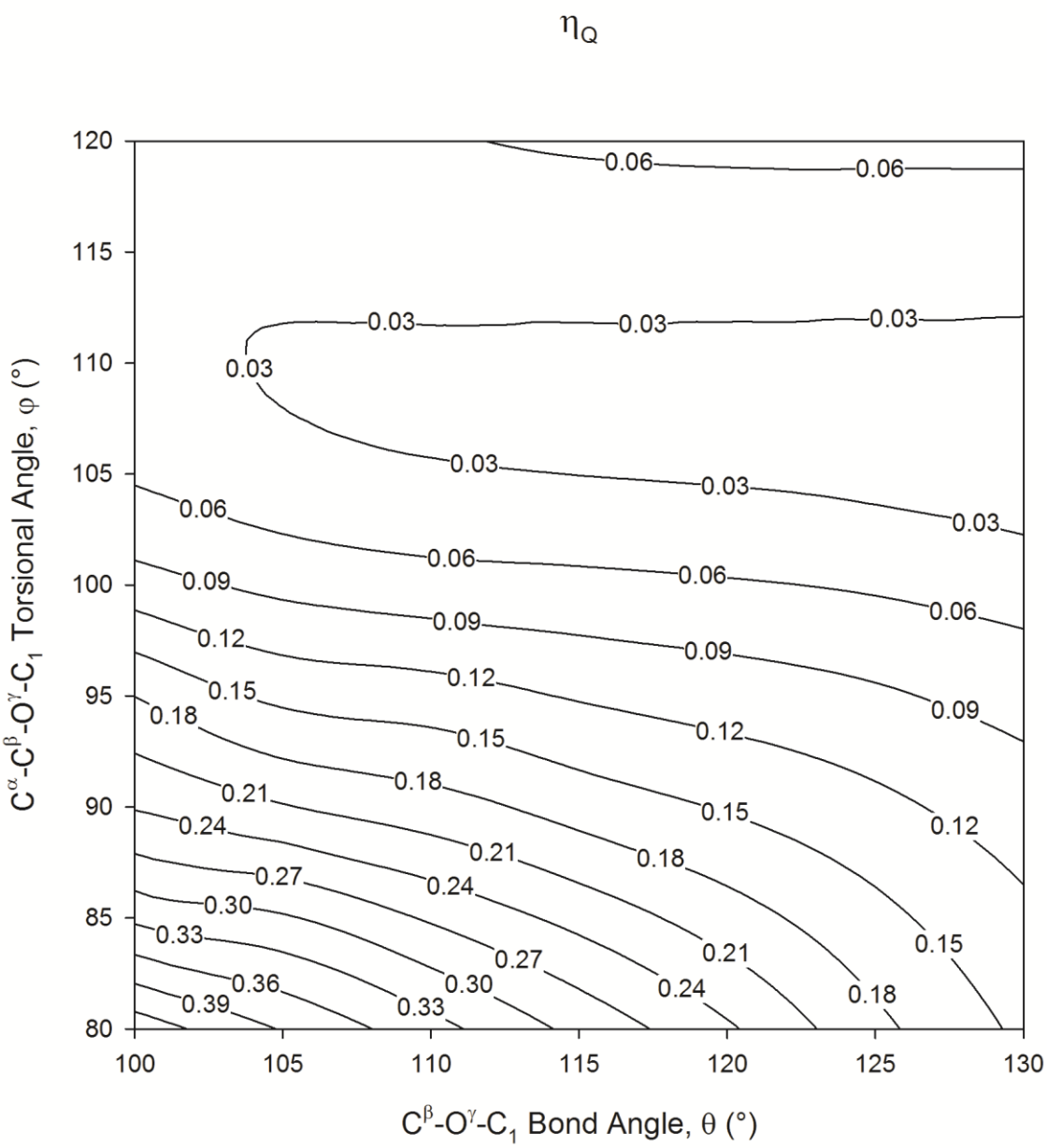

Figure A- 7: Computed asymmetry parameter (η_Q) of the electric field gradient tensor of selected residues of acetyl-γ-chymotrypsin.

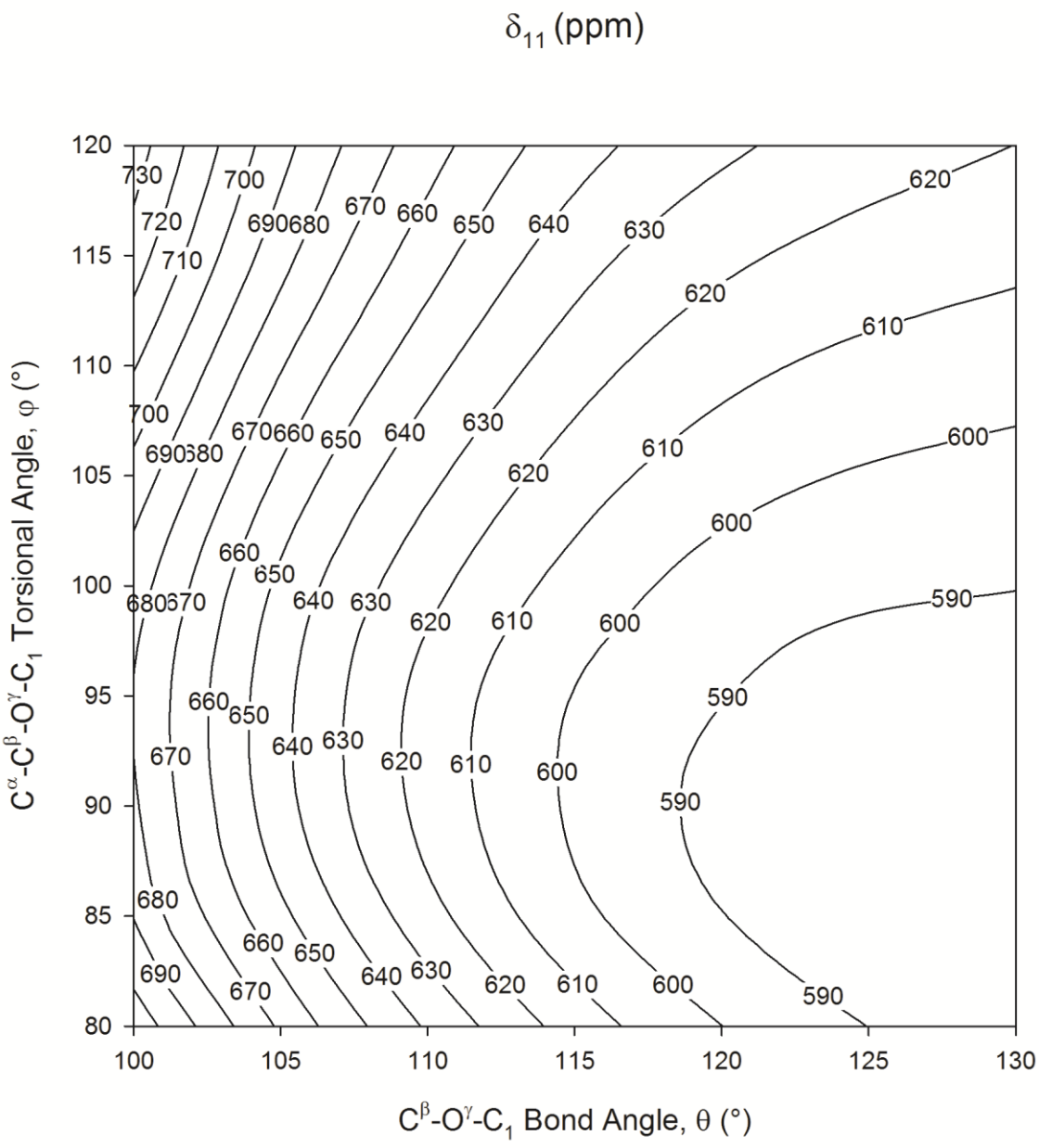

Figure A- 8: Computed chemical shift tensor component δ_{11} of selected residues of acetyl-γ-chymotrypsin.

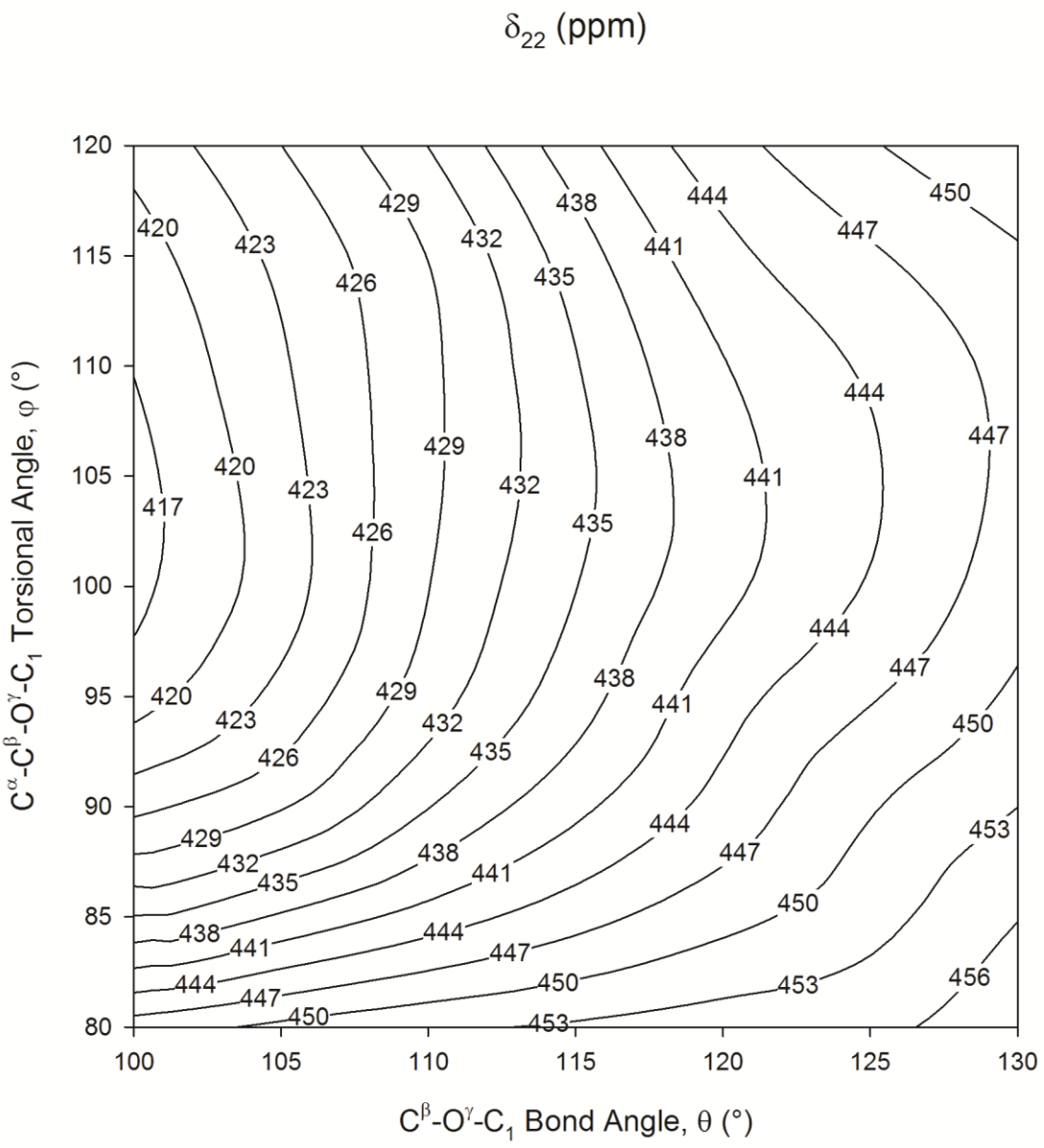

Figure A- 9: Computed chemical shift tensor component δ_{22} of selected residues of acetyl-γ-chymotrypsin.

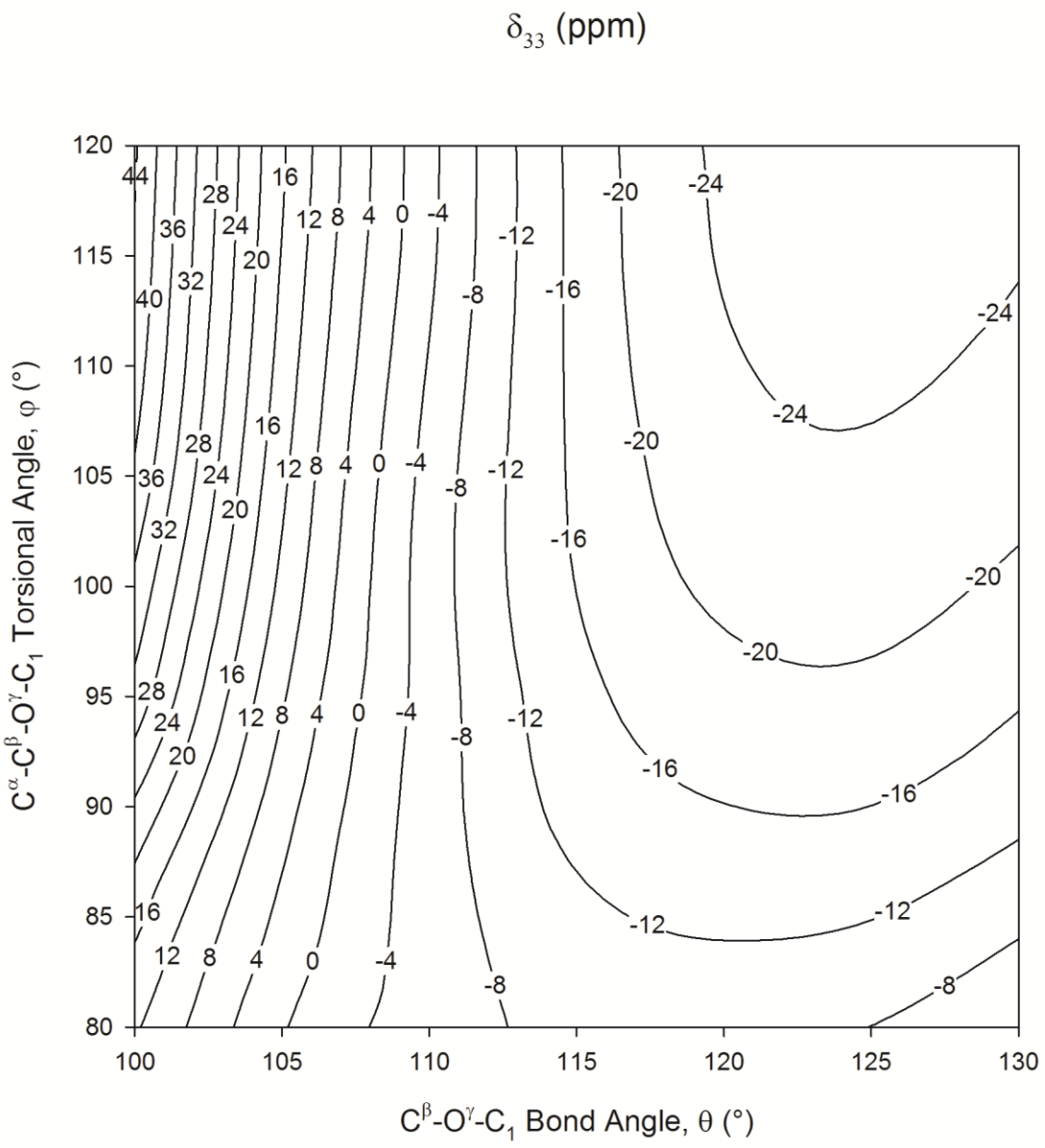

Figure A- 10: Computed chemical shift tensor component δ_{33} of selected residues of acetyl-γ-chymotrypsin.

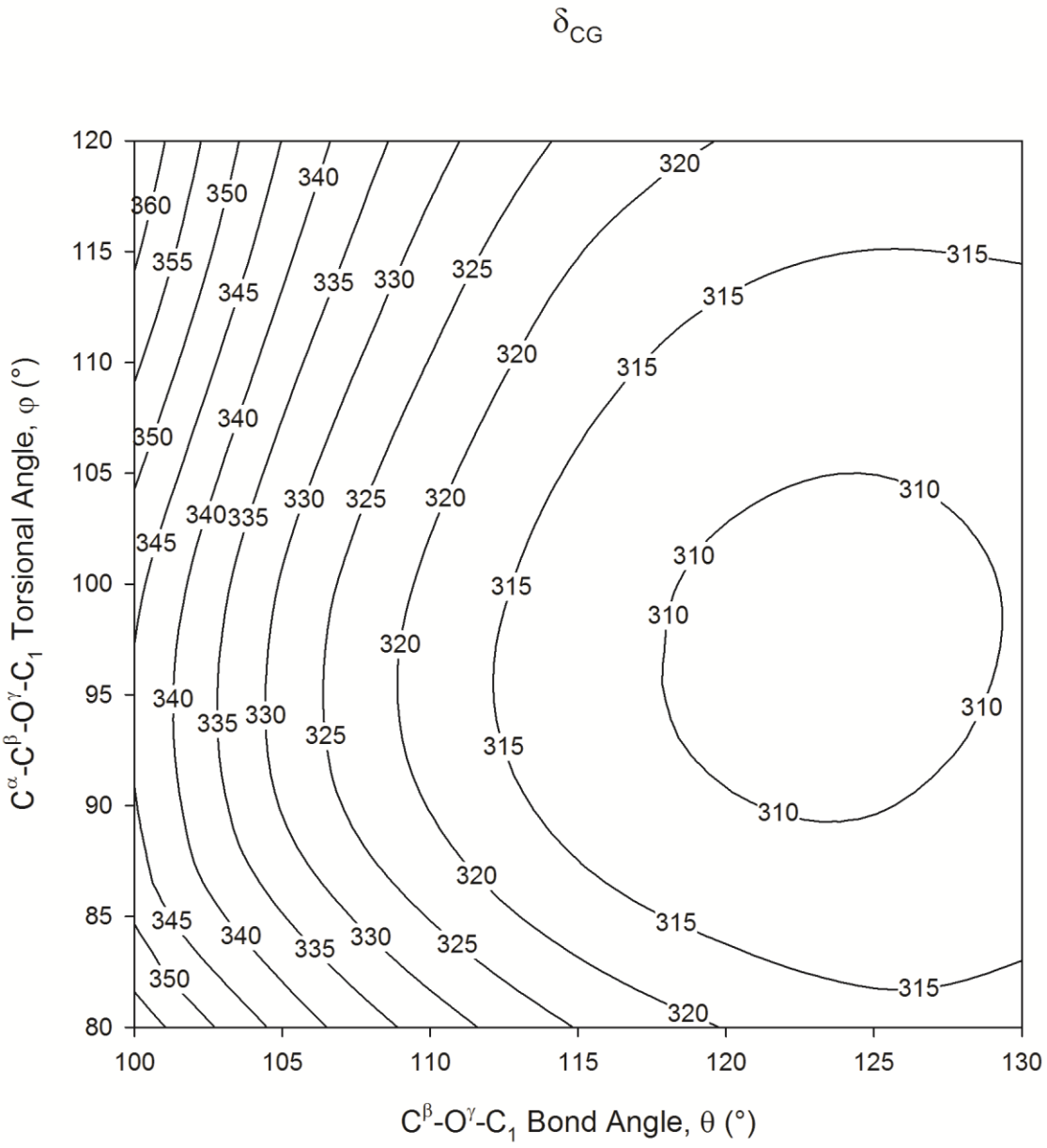

Figure A- 11: Computed center of gravity, δ_{CG}, of selected residues of acetyl-γ-chymotrypsin.